VELOCITY EFFECTS IN TRANSVERSE MODE LIQUID PROPELLANT ROCKET COMBUSTION INSTABILITY[1]

BY

F. H. Reardon[2], L. Crocco[3], and D. T. Harrje[4]

Princeton University

1. This work was sponsored by the National Aeronautics and Space Administration under grant NsG 99-60 and previously under joint sponsorship with the Bureau of Naval Weapons, U.S. Navy, under contracts $NO_{as}60$-6078-C and $NO_{w}61$-0686-d.

2. Presently Supervisor, Combustion Dynamics, Thrust Chamber Department, Liquid Rocket Plant, Aerojet-General Corporation, Sacramento, Calif. Member AIAA.

3. Robert H. Goddard Professor of Aerospace Propulsion and Space Flight. Fellow Member AIAA.

4. Research Aeronautical Engineer, Associate Fellow Member AIAA.

ABSTRACT

Analytical and experimental studies have confirmed the application of the pressure-sensitive combustion time lag to transverse as well as longitudinal modes of high frequency combustion instability in liquid propellant rocket engines. However, a recent series of tests at Princeton University has demonstrated that an additional combustion rate sensitivity must be considered in the transverse mode case. In the present paper, the theory of transverse mode combustion instability is extended to include linearized velocity effects. Fluctuations of the radial and tangential velocity components are assumed to influence the combustion process rates in a manner analogous to that previously proposed by Crocco for pressure perturbations. A physical mechanism is suggested in the enhancement of the reactant mixing which can be affected by the transverse components of the gas velocity. The analysis predicts that the tangential velocity perturbation may have a strong destabilizing effect on spinning tangential modes but will have no effect on standing modes. The radial velocity fluctuation is shown to have a smaller but significant influence. Experimental verification of the predicted effects has been obtained for a fuel-on-oxidizer impinging doublet injector pattern and for like-on-like injection using close spacing (0.1") of the liquid spray fans.

I. INTRODUCTION

High frequency combustion instability remains one of the most critical problems in the development of liquid propellant rocket engines. This phenomenon consists of a forced oscillation of the combustion chamber gases, driven by the combustion process interacting with the resonance effects of the chamber geometry. The resulting oscillation patterns are very similar to those of the acoustic modes of the chamber. For a cylindrical chamber, closed at both ends one can distinguish between longitudinal and transverse acoustic modes. In a longitudinal mode the property variations occur in the axial direction, whereas conditions are uniform on a section normal to the axis. Purely transverse modes involve uniformity of the properties along the axis but variations in the radial and circumferential directions. The transverse modes can be further classified into tangential, radial, and combined tangential-radial modes (see Reference 1). It has been observed that the frequencies of fully developed transverse mode combustion oscillations fall within a few percent of the acoustic frequencies of the corresponding modes. Each tangential mode can exist in two forms, the standing form, in which the nodal surfaces are stationary; and the spinning form, in which the nodal surfaces rotate at the angular frequency of the oscillation. The two forms of the first tangential mode are illustrated in Figure 1, which shows, schematically, pressure and velocity patterns at four instants during a period of oscillation.

Analytical and experimental studies (1-4) have confirmed the application of the pressure sensitive combustion time lag concept to transverse as well as longitudinal modes of high frequency instability. However, a recent series of tests at Princeton University has demonstrated that an additional combustion rate sensitivity must be considered in the transverse mode case (5). These

tests used a simple fuel-on-oxidizer impinging doublet injector, with 12 injection points equally spaced about the circumference of a single circle. Each doublet pair was contained in a single "spud", which could be oriented in either of two ways, 90° apart (see Figure 2). In the "radial" orientation, each spud was arranged so that the line of centers of the injector orifices lay along a radius. With the spud in the "tangential" orientation, the line of centers was tangential to the injection circle. Typical test results are shown in Figure 3, in which the test points are plotted on the chamber pressure, mixture ratio plane, with the nature of the oscillation shown by the shading of the point. All tests with the tangential orientation were unstable in the first tangential mode. However, quite different results were obtained with the radial orientation. In general, the latter were more stable; some thrust chamber configurations gave complete stability for all operating conditions. Such effects have been reported previously by other investigators (6, 7). It is generally agreed that the explanation for injection spray orientation effects should be based on the sensitivity of the liquid propellant combustion process to fluctuations of the transverse gas velocity or displacement components.

The analysis which follows is based on the consideration of the stability of small perturbations. Each of the quantitles describing the flow in the rocket motor is assumed to oscillate about a given steady-state value. For certain operating conditions, the oscillation amplitudes will increase with time, even for arbitrarily small initial amplitudes. Since random fluctuations of small but finite amplitude (generally referred to as "combustion noise") are always present in a rocket motor, such unstable operating conditions must be avoided. The approach which will be used in the determination of the stability of a rocket combustion system is the follow-

ing. Conditions will be established for the existence of neutral oscillations, the amplitudes of which neither increase nor decrease with time. The assemblage of the operating points of the system which satisfy the conditions for neutral oscillation form the "stability limits" which divide the unstable from the stable regions of operation. The complete stability behavior of the rocket is described by specifying the stability limits and indicating the unstable regions.

The rocket motor to be considered consists of a circular cylindrical combustion chamber of length L_c and radius r_c, followed by a converging-diverging expansion nozzle. The wallsare assumed to be rigid, impervious, and perfectly insulating. The medium within the chamber consists of gaseous products of combustion in which are distributed burning droplets of the liquid propellants. The volume occupied by the liquid is taken to be negligibly small. In this two phase flow, the burning droplets act as distributed sources of mass, momentum, and energy. It is assumed that combustion is completed within the combustion chamber and that the gas velocity in the chamber is so small that the square of the Mach number is negligible compared to unity. Thus, in this ideal rocket motor, the flow is divided into two parts, a low speed combustion process and an expansion to supersonic velocity without combustion.

It is convenient to carry out the analysis in terms of the following dimensionless variables:

$$\text{pressure} \quad p = \frac{p^*}{p_0^*}$$

$$\text{density} \quad \rho = \frac{\rho^*}{\rho_0^*} \qquad (1)$$

$$\text{temperature} \quad T = \frac{T^*}{T_0^*}$$

$$\text{enthalpy} \quad h = \frac{(\gamma-1)h^*}{\gamma R^* T_0^*} = \frac{h^*}{c_p^* T_0^*}$$

$$\text{entropy} \quad s = \frac{s^*}{c_p^*}$$

velocity $\vec{V} = \frac{\vec{V}^*}{\bar{c}_o^*}$

mass burning rate per unit volume $Q = \frac{Q^* r_c^*}{\bar{\rho}_o^* \bar{c}_o^*}$

time $t = \frac{t^* \bar{c}_o^*}{r_c^*}$ (1)

axial distance $z = \frac{z^*}{r_c^*}$

radial distance $r = \frac{r^*}{r_c^*}$

where c^* is the velocity of sound, c_p^* is the constant pressure specific heat, $\gamma = \frac{c_p^*}{c_v^*}$ is the ratio of specific heats, and R* is the gas constant. The subscript o denotes values at the injector face ($z=0$),* indicates a dimensional quantity, a superposed arrow indicates a vector, and barred quantities correspond to steady-state. Droplet properties will be denoted by the subscript L. According to the avove definitions ρ_L^* is not the actual droplet density but rather the total mass of droplets per unit volume of gas. Since the steady-state gas velocity must vanish at the injector face, $\bar{p}_o^*$, $\bar{\rho}_o^*$, $\bar{T}_o^*$ and $\bar{c}_o^*$ are stagnation quantities.

Each quantity is written as the sum of a steady-state part and a time varying perturbation. Thus the pressure is expressed as

$$p = \bar{p} + p' e^{st} \qquad (2)$$

where $\bar{p}$ is the steady-state pressure and p' is the complex, space dependent perturbation amplitude. (For simplicity in the analysis below the term "pressure perturbation" will be understood to mean p' only). In the time dependent factor e^{st}, $s = \lambda + i\omega$ in which the real part λ is the amplification factor and the imaginary part ω is the frequency of oscillation.* The condition $\lambda = 0$ corresponds to neutral oscillation at a stability

* In the complex representation of oscillation quantities, used in this analysis, the actual physical value of a quantity is given by the real part of the corresponding complex expression.

limit, while $\lambda<0, \lambda>0$ represent stability and instability, respectively. As mentioned above, the analysis will be directed toward the determination of the conditions which prevail when $\lambda=0$ or $s=i\omega$. It is assumed, as usual, that the perturbations are so small that the squares and products of perturbations can be neglected in comparison to the steady-state values. This procedure leads to a set of 10 simultaneous, linear, partial differential equations for the perturbations of pressure, velocity, etc., which are detailed in Reference 5.

II. VELOCITY-OR DISPLACEMENT-SENSITIVE BURNING RATE

The system of perturbation equations is not complete without an expression for the burning rate perturbation, $\dot{Q}'$. The relation for $\dot{Q}'$ derived by Crocco (2) and later used by Scala (3) made use of the concept of the combustion time lag. That is, the gradual evolution of combustion products from an element of propellant mixture traveling through the combustion chamber after injection was approximated by a discontinuous conversion from reactants to products after a certain time, called the time lag, had elapsed. By this approximation, the impossible task of describing the combustion process through the quantitative knowledge of its intermediate history was greatly simplified. It was recognized that if the combustion chamber conditions fluctuate, the time lag must also vary. An additional approximation was introduced to simplify the description of the effect of the chamber conditions on the time lag. The total time lag τ_T was taken as the sum of an insensitive time lag τ_i , and a sensitive time lag τ . The various physical conditions were assumed to affect the combustion processes only during the sensitive portion of the total time lag. Thus, during fluctuating operation of the rocket motor, the time variation of the total combustion time lag is taken up completely by the sensitive time lag; the insensitive

time lag is constant.

In the following analysis, attention will be concentrated on intrinsic instability, that is, instability occurring when the injection rate is constant. Then the burning rate perturbation is related to the rate of change of the time lag by the expression

$$Q' e^{st} = Q - \bar{Q} = -\frac{d\bar{u}}{dz}\frac{d\tau}{dt} \qquad (3)$$

where $\frac{d\bar{u}}{dz} = \bar{Q}$ is the steady-state combustion intensity. Spatial effects due to the fluctuations of the total time lag and liquid droplet velocity contribute terms of the same order of magnitude as $\bar{u}\frac{d\bar{u}}{dz}$. While $\frac{d\bar{u}}{dz}$ may be O(1)* locally, the effect of this factor integrated over the entire chamber is only $O(\bar{u}_e)$, where $\bar{u}_e$ is the dimensionless velocity at the nozzle entrance. This result is demonstrated in Reference 5. The terms introduced by spatial variations are therefore $O(\bar{u}_e^2)$ and have been neglected.

In the original formulation by Crocco, the time lag was defined by assuming that the transformation to burned gases takes place only when the processes occurring during the time lag have accumulated up to a well determined level, $\bar{E}_a$. This condition was expressed by the equation

$$\int_{t-\tau_\tau}^{t} f[\tau_i(t')]dt' = \bar{E}_a = \int_{t-\bar{\tau}_\tau}^{t} \bar{f}[\tau_i(t')]dt' \qquad (4)$$

were f is the overall rate of the various processes involved in the combustion of the liquid bipropellants, and t is the time at which the transformation to burned gases occurs. In the integrals, the rate f

*As usual the symbol O(x) means "of the same order or magnitude as x".

must be computed using the instantaneous values of the physical conditions at each instant t' at the location x_i (representing the spatial variables z, r, θ) where the element is at that instant. The sensitivity of the rate f to variations in chamber conditions (correlated to the local pressure) was expressed by the interaction index n, defined by

$$n = \frac{\bar{p}}{\bar{f}}\left(\frac{\partial f}{\partial p} + \frac{\partial f}{\partial T}\frac{\partial T}{\partial p} + \cdots\right) \qquad (5)$$

where the parenthetical expression is evaluated at the steady-state operating conditions. The assumption was made that the sensitive portion of the time lag occurs just before the conversion to combustion products. Then during the insensitive time lag the unsteady process rate is equal to the steady-state rate,

$$f = \bar{f}, \qquad t - \tau_T \le t' \le t - \tau \qquad (6)$$

Since the unsteady pressure is of the form $p = \bar{p} + p' e^{st}$, the process rate during the sensitive time lag is given by

$$f = \bar{f}\left(1 + n p' e^{st'}\right), \qquad t - \tau \le t' \le t \qquad (7)$$

Making use of these relations, the burning rate perturbation was found to be given by

$$Q' = \frac{d\bar{u}}{dz}\, n \left\{1 - \frac{p'[r_i(t-\bar{\tau})]}{p'[r_i(t)]} e^{-s\bar{\tau}}\right\} p'[r_i(t)] \qquad (8)$$

which is of the form

$$Q' = \frac{d\bar{u}}{dz} \mathcal{P}_{p'}[x_i(t)] \qquad (9)$$

In the derivation of this burning rate expression, it was assumed that all quantities affecting the combustion process could be correlated to the local pressure. While this assumption can be applied to thermodynamic state properties such as temperature and density, it can not be applied to the components of the gas velocity, which may be of equal importance in the combustion process. The effects of the velocity perturbations must therefore be taken into account separately from the effects of those quantities which can be correlated with the pressure.

Only the transverse (i.e., radial and tangential) components of the velocity perturbation can be significant in the explanation of the orientation effect described above. For purely transverse modes of oscillation, the longitudinal component is always much smaller than the transverse components. In addition, the longitudinal velocity perturbation vanishes at the injector face and has its smallest magnitude in the early combustion region, the zone in which baffles have been seen to have the greatest influence on stability.

Of the various intermediate processes occurring during the combustion of liquid bipropellants, those most sensitive to velocity are the vaporization of the liquid droplets and the mixing of the vaporized propellants which must precede chemical reaction. In the process of vaporization, the important quantity is the absolute magnitude of the velocity of the hot gases relative to the liquid droplet. The differences in the velocity patterns of the standing and spinning forms of tangential modes of oscillation (which were observed to have strikingly different stability charac-

teristics) could result in differences in the local and overall vaporization rates. However, since the direction of the relative velocity is immaterial, the orientation effect is not explainable by means of the vaporization process. In addition, the theoretical sutdy of Wieber and Mickelsen (8) indicates that the oscillating velocity effect on droplet vaporization is essentially nonlinear because of the dependence of the evaporation rate on the absolute magnitude of the relative velocity. On the other hand, for our injector configuration, the mixing of the propellants by the oscillating velocities may be linearized and is very strongly dependent on the orientation of the liquid spray fans (produced by the fuel-on-oxidizer impinging doublet injector). Although no detailed description of such a complex phenomenon is now possible, the following schematic discussion illustrates one process by which the burning rate may be caused to oscillate by an oscillating transverse velocity.

Consider the mixture of gaseous combustion products, vaporized propellants (oxidizer and fuel), and liquid propellant droplets at some axial station downstream of an injector doublet. For an fuel-on-oxidizer impinging injector, liquid mixing is imperfect and some degree of stratification exists in the mixture (9). For concreteness, the area of interest is shown in Figure 4 (a) for a doublet spud oriented with the line of centers of its orifices tangential to the injection circle. Then the stratification is almost entirely in the tangential direction, as shown by the lines of constant mass fraction of vaporized oxidizer in the gas mixture, Y_x. The exact shape of the constant Y_x contours will be dependent on the design and operating mixture ratios, the propellant characteristics, etc. Because of the turbulence in the combustion chamber, the stratification pattern shown schematically in Figure 4 (a) represents only mean conditions.

Assume first that the rates of evaporation of the two propellants are comparable. A typical fuel rich droplet is shown at position A in the region which is relatively rich in vaporized fuel. A corresponding oxidizer rich droplet is shown at B in the oxidizer rich region of the mixture. As a droplet evaporates, the vapors diffuse away and must mix* with the other vaporized propellant in the proper proportions for chemical reaction. The overall burning rate of a fuel rich droplet, will therefore be a function of the amount of oxidizer vapor near the droplet.

In the presence of small, periodic, transverse gas velocity oscillations ($v'e^{i\omega t}, w'e^{i\omega t}$), the gaseous mixture will be displaced relative to the droplets, causing oscillations of the local mass fractions of oxidizer and fuel. The motion of the larger droplets is small compared to the gas motion, while the smaller droplets tend to move with the gas. Therefore the discussion here pertains to the larger droplets. As a droplet evaporates, it tends to be displaced with the gas and the effect of the transverse velocity on its burning rate decreases. Thus the velocity effect described here can be expected to be most important in the early combustion region, in agreement with experimental results. Since the fuel rich droplet is in an oxidant deficient region, an increase in the oxidizer mass fraction will increase its contribution to the overall burning rate. The opposite is true for the oxidizer rich droplet; an increase in the local oxidizer fraction is accompanied by a decrease in the local fuel fraction. Thus, a perturbation velocity, or a displacement, in the positive θ-direction (see Figure 4(a)) will increase the oxidizer rich droplet burning rate and decrease the fuel rich droplet burning rate. Therefore the effects on the two droplets will tend to cancel where the two propellants have comparable evaporation rates. Of

* In a rocket combustion chamber, the transport and mixing of the vapors is most likely to be carried out primarily by turbulence rather than molecular diffusion.

course, in order to determine the effect of the velocity perturbation of the entire spray, all of the propellant droplets must be considered.

Let us now consider the case when one of the propellants, e.g., the oxidizer, vaporizes at a greater rate than the other. In that case there will be very little fuel vapor in the early stages where oxidizer droplets are evaporated, and practically no oxidizer droplets left in the latter stages where fuel vapor is being produced. Therefore, there will be less cancellation of opposing effects and the overall velocity effect will be determined by the burning of the droplets of the fuel in the surrounding gas containing a non uniform oxidizer vapor concentration. Indeed, for the liquid oxygen-ethyl alcohol combination used in the instability experiments at Princeton University, it can be estimated, using the spray evaporation calculations of Priem and Heidmann (10) and the relative vaporization rate data of Pass and Tischler (11), that at any early station, twice as much oxidant as fuel will have evaporated. Thus important velocity or displacement effects can be expected. For other propellant combinations, the evaporation rates of the fuel and oxidizer could be quite similar, and hence the velocity mixing effect could be considerably reduced.

If the injector doublet which produces the mixture discussed above is rotated through an angle β_i from the tangential orientation, the resulting mixture will also be rotated, and will appear as shown in Figure 4(b). Therefore, the net combustion process rate perturbation will in general depend on both the radial and tangential velocity (or displacement) components and can be written in the form

$$f' = (\ell_r v' + \ell_\theta w') e^{i\omega t} \qquad (9a)$$

where ℓ_r and ℓ_θ are radial and tangential

velocity interaction indices analogous to the pressure interaction index defined originally by Crocco (equation (5). Here we have chosen to represent the burning rate perturbation in terms of the velocity components, because these are among the dependent variables appearing in the treatment that follows. This formulation, however, covers also the case when the relevant parameters are the components $\delta_r' e^{i\omega t}$ and $\delta_\theta' e^{i\omega t}$ of the displacement. Indeed we have

$$\frac{d}{dt}\left(\delta_2' e^{i\omega t}\right) = i\omega\delta_r' e^{i\omega t} = v' e^{i\omega t}; \quad \frac{d}{dt}\left(\delta_\theta' e^{i\omega t}\right) = i\omega\delta_\theta' e^{i\omega t} = w' e^{i\omega t}$$

so that equation (9a) can be written

$$f' = \left(m_r \delta_r' + m_\theta \delta_\theta'\right) e^{i\omega t} \tag{9b}$$

with

$$m_r = i\omega \ell_r \quad , \quad m_\theta = i\omega \ell_\theta \tag{9c}$$

If the displacement interaction indices m_r and m_θ were real and constant, the corresponding velocity interaction indices would be imaginary and frequency dependent. In all cases the displacement indices present a 90° phase shift with respect to the velocity indices.

Keeping in mind the relations (9c), the expression (9a) for f' can be used in all cases, and from now on we shall speak only of velocity effects, including in this expression also the effects that should more directly be attributed to the displacement.

It must be clear that the above linearized expressions will not be valid for all types of injection patterns and that non-linear effects will often be present. For example, approximately linear effects can be expected with the

fuel-on-oxidizer impinging doublet and for the like-on-like pattern if the spacing between unlike fans is sufficiently small. However, for large spacings, non-linear velocity or displacement effects should be taken into consideration.

At the present time, the magnitudes of the velocity indices and their variations with axial distance cannot be calculated because of the lack of quantitative knowledge of the processes involved in liquid propellent combustion under turbulent conditions. From an heuristic point of view, we shall in this paper only consider two particularly simple expressions. One comes from the assumption that the velocity effects occur during the same time interval (the sensitive time lag) as the pressure effects. Assuming, then, a linear dependence of the perturbation of the overall rate of the processes occurring during the sensitive time lag on the perturbation of pressure and radial and tangential velocity, equation (7) becomes

$$f(t') = \left(1 + n p' e^{st'} + l_r v' e^{st'} + l_\theta w' e^{st'}\right) \bar{f}, \quad t - \bar{\tau} \leq t' \leq t \tag{10}$$

The time rate of change of the sensitive time lag is found, by the same procedure as used previously to be

$$\frac{d\tau}{dt} = -n p'[r_i(t)] e^{st} \left\{ 1 - \frac{p'[r_i(t-\bar{\tau})]}{p'[r_i(t)]} e^{-s\bar{\tau}} \right\} - l_r v'[r_i(t)] e^{st} \left\{ 1 - \frac{v'[r_i(t-\bar{\tau})]}{v'[r_i(t)]} e^{-s\bar{\tau}} \right\} - l_\theta w'[r_i(t)] e^{st} \left\{ 1 - \frac{w'[r_i(t-\bar{\tau})]}{w'[r_i(t)]} e^{-s\bar{\tau}} \right\} \tag{11}$$

Then burning rate perturbation can be written as

$$Q' = \frac{d\bar{u}}{dz} \mathcal{P} p'[\eta_i(t)] + \frac{d\bar{u}}{dz} \mathcal{R} v'[\eta_i(t)] + \frac{d\bar{u}}{dz} \mathcal{J} w'[\eta_i(t)] \quad (12)$$

where

$$\mathcal{P} = n \left\{ 1 - \frac{p'[\eta_i(t-\bar{\tau})]}{p'[\eta_i(t)]} e^{-s\bar{\tau}} \right\} \quad (12a)$$

$$\mathcal{R} = l_r \left\{ 1 - \frac{v'[\eta_i(t-\bar{\tau})]}{v'[\eta_i(t)]} e^{-s\bar{\tau}} \right\}$$

$$\mathcal{J} = l_\theta \left\{ 1 - \frac{w'[\eta_i(t-\bar{\tau})]}{w'[\eta_i(t)]} e^{-s\bar{\tau}} \right\}$$

In general, $\bar{\tau} = \bar{\tau}(z)$ varies from one propellant element to another. The effect on combustion instability of such a spread in the sensitive time lag has been evaluated by Crocco and Cheng (1). In this analysis, it is assumed that all propellant elements have equal mean sensitive time lags, so that $\bar{\tau}$ = constant. It must be observed here that this formulation applies equally to the case when the value of $\bar{\tau}$ is different for the pressure and the velocity effects. Consideration is given to this and other formulations in Reference 5. It should be noted, however, that these alternative formulations involve additional perimeters which cannot be calculated a prior and which would produce quite a problem if they were to be determined from empirical obstruction. Moreover, the quantitative consideration of possible interaction mechanisms (to be discussed in a future paper) gives weight to the hypothesis of equal sensitive time lags.

Another simple expression for the burning rate is again inspired by the qualitative examination of possible interaction mechanisms, which shows that it is possible for a part of the burning rate variation to be in phase with the variation of concentration of the more volatile propellant, and hence with

the displacement itself. In this case the coefficients of (9b) are real and those of (9a) imaginary. The resulting expression for Q' is still given by (12), with $\mathcal{P}$ still provided by (12a), but $\mathcal{R}$ and $\mathcal{J}$ given by the simple expressions

$$\mathcal{R} = \frac{m_r}{i\omega} \quad , \quad \mathcal{J} = \frac{m_\theta}{i\omega} \qquad (12b)$$

III. SOLUTION FOR THE PERTURBATIONS

The addition of velocity terms to the burning rate perturbation expression makes separation of the variables, as used in Reference (3), impossible. Therefore a different approach is used. The solutions assumed to take the form of a series; the pressure perturbation, for example is

$$p' = p_0 + p_1 + p_2 + \cdots \qquad (13)$$

where p_1 is assumed to be $O(\bar{u}_e p_0)$, p_2 is $O(\bar{u}_e^2 p_0)$, etc. Since the governing equations were derived neglecting terms of $O(\bar{u}_e^2)$, the solution will be carried only as far as the first order correction, p_1. As discussed previously, it is assumed that the combustion process produces an unperturbed velocity in the combustion chamber, which is small compared to the velocity of sound; and that the droplet drag, (and hence the droplet oscillation amplitude), is also small. Therefore, the zeroth order solution corresponds to acoustic oscillations, and the first order correction includes the effects of the combustion process, the liquid gas interaction, and the exhaust nozzle.

Following this procedure, the perturbation equations can be expressed as follows (see Ref. (5)):

$$\Delta p_0 - s^2 p_0 = 0 \tag{14}$$

$$\Delta p_0 - s^2 p_1 = \left[R' \bar{\rho}_2 + (\gamma+1)\frac{d\bar{u}}{dz}\right] s p_0 - \gamma s \mathcal{P} \frac{d\bar{u}}{dz} p_0 + R \frac{d\bar{u}}{dz} \frac{\partial p_0}{\partial r} + J \frac{d\bar{u}}{dz} \frac{1}{r} \frac{\partial p_0}{\partial \theta}$$

where Δ is the Laplacian operator

$$\Delta = \frac{\partial^2}{\partial z^2} + \frac{\partial^2}{\partial r^2} + \frac{1}{r}\frac{\partial}{\partial r} + \frac{1}{r^2}\frac{\partial^2}{\partial \theta^2}$$

The boundary conditions at the combustion chamber wall are that the velocity perturbation normal to the wall must vanish; that is, $u' = 0$ at $z = 0$ and $v' = 0$ at $r = 1$. In addition, it is necessary to impose conditions of boundedness and periodicity in order to obtain a solution. At the combustion chamber exit, $z = z_e$, the proper boundary condition is a relation between the perturbations of pressure, velocity, and entropy.

For transverse modes, the zeroth order solution has been found to be

$$p_0 = p_\infty \left[1 + (s^2 + s_{\gamma h}^2)\frac{z^2}{2}\right] \Psi_{\gamma h}(r)\, \Theta_\gamma(\theta) \tag{15}$$

correct to terms of the order of the chamber exit Mach number, $\bar{u}_e$.

In equation (15)

$$\Psi_{\gamma h}(r) = J_\gamma(s_{\gamma h} r)$$

and

$$\Theta_\gamma(\theta) = \cos \gamma\theta \qquad \text{(standing mode)} \tag{16}$$

or $\Theta_\nu(\theta) = e^{-i\nu\theta}$ (spinning mode)(*)

Each value of the constant $s_{\nu h}$ is characteristic of a mode of oscillation. Physically, h is the number of cylindrical surfaces, including the outer solid wall, on which the radial velocity perturbation vanishes; h = 1 corresponds to a purely tangential mode, h = 2 to the first radial mode, h= 3 to the second radial mode, etc. The standing mode tangential velocity perturbation vanishes on stationary diametral surfaces (nodal surfaces) which can then be replaced by solid surfaces (e.g., baffles or sector inserts, Ref. (1)) without disturbing the oscillation pattern. In a spinning mode the nodal surfaces rotate at the oscillation frequency. For $\nu = 0$, the θ solution is simply

Θ_0 = Constant = 1

which represents a purely radial mode, since there is no variation in the tangential direction. The first tangential mode corresponds to ν = 1, the second tangential mode to ν = 2, and so on.

The second order solution can be found by superposition. Let

$$P_1 = P_A + P_B + P_C + P_D \tag{17}$$

where the partial solutions P_A, P_B, P_C and P_D are solutions of the following equations

$$\Delta P_A - s^2 P_A = -\gamma s \mathcal{P} \frac{d\bar{u}}{dz} P_{00} \Psi_{\nu h} \Theta_\nu \tag{18a}$$

$$\Delta P_B - s^2 P_B = \mathcal{R} \frac{d\bar{u}}{dz} P_{00} \frac{d\Psi_{\nu h}}{dr} \Theta_\nu \tag{18b}$$

$$\Delta P_C - s^2 P_C = \mathcal{T} \frac{d\bar{u}}{dz} P_{00} \frac{\Psi_{\nu h}}{r} \frac{d\Theta_\nu}{d\theta} \tag{18c}$$

(*) This expression corresponds to spinning in the positive θ direction. Spinning in the opposite direction would be represented by $\exp(i\nu\theta)$ or can simply be taken care of by changing the positive θ direction.

$$\Delta p_D - s^2 p_D = \left[k'(z)\bar{p}_2(z) + (\gamma+1)\frac{d\bar{u}}{dz} \right] s\, P_{oo}\, \Psi_{\nu h}\, \Theta_\nu \qquad (18d)$$

It is seen that the pressure sensitive combustion effects appear in p_A, and the radial and tangential velocity sensitivities enter into p_B and p_C, respectively. The partial solution p_D includes the effect of the liquid droplet drag.

The partial solution p_A can be obtained by letting

$$p_A = P_A(z)\, \Psi_{\nu h}(r)\, \Theta_\nu(\theta) \qquad (19)$$

then equation (18a) becomes

$$\frac{d^2 P_A}{dz^2} \Psi_{\nu h} \Theta_\nu + P_A \left(\frac{\partial^2}{\partial r^2} + \frac{1}{r}\frac{\partial}{\partial r} + \frac{1}{r^2}\frac{\partial^2}{\partial \theta^2} \right) \Psi_{\nu h} \Theta_\nu - s^2 P_A \Psi_{\nu h} \Theta_\nu = -\gamma_s P \frac{d\bar{u}}{dz} P_{oo} \Psi_{\nu h} \Theta_\nu \qquad (20)$$

The transverse distribution function satisfy the relation

$$\left(\frac{\partial^2}{\partial r^2} + \frac{1}{r}\frac{\partial}{\partial r} + \frac{1}{r^2}\frac{\partial^2}{\partial \theta^2} \right) \Psi_{\nu h} \Theta_\nu = -s_{\nu h}^2\, \Psi_{\nu h}\, \Theta_\nu \qquad (21)$$

Making use of this relation, equation (20) becomes

$$\frac{d^2}{dz^2}\left(\frac{P_A}{P_{oo}}\right) + \left(s^2 + s_{\nu h}^2\right)\left(\frac{P_A}{P_{oo}}\right) = -\gamma_s P \frac{d\bar{u}}{dz} \qquad (22)$$

However, since $s^2 + s_{\nu h}^2$ and $\frac{P_A}{P_{oo}}$ are both $O(\bar{u}_e)$, the differential equation for P_A reduces to

$$\frac{d^2}{dz^2}\left(\frac{P_A}{P_{oo}}\right) = -\gamma_s P \frac{d\bar{u}}{dz} + O(\bar{u}_e^2) \qquad (23)$$

This equation is easily integrated to give

$$\frac{P_A(z)}{P_{oo}} = -\gamma_s P \int_0^z \bar{u}(z')\, dz' + K_A \qquad (24)$$

where the integration constant K_A represents the value of $\frac{P_A}{P_{oo}}$ at the injector face, $z = 0$; therefore, $K_A = O(\bar{u}_e)$.

The partial solution φ_D is obtained in the same manner from equation (18D) with $\varphi_D = P_D(z)\,\Psi_{ph}(r)\,\omega_j(\theta)$ and

$$\frac{P_D}{P_{oo}} = s\int_0^z dz' \int_0^{z'} k'(z'')\,\bar{\rho}_L(z'')\,dz'' + (\gamma+1)s\int_0^z \bar{u}(z')\,dz' + K_D \qquad (25)$$

where again

$$K_D = \frac{P_D(0)}{P_{oo}} = O(\bar{u}e).$$

A different procedure must be adopted in order to obtain the partial solutions φ_B and φ_C because equations (18B) and (18C) are not separable. These equations are of the form

$$\Delta p - s^2 p = F(z)\,G(r,\theta) \qquad (26)$$

The solutions (eigenfunctions) of the corresponding homogeneous equation are

$$\Psi_{pq}(r) = J_p(s_{pq}r) \qquad (27)$$

$$\omega_p(\theta) = \cos p\theta \quad \text{or} \quad e^{-ip\theta}(*)$$

$$p = 0, 1, 2, 3 \cdots \; ; \; q = 1, 2, 3, \cdots$$

These transverse eigenfunctions form a complete, orthogonal set. A solution of equation (26) can be obtained, therefore, by expanding $G(r,\theta)$ in a series of the transverse eigenfunctions.**

$$G(r,\theta) = \sum_{p=0}^{\infty}\sum_{q=1}^{\infty} A_{pq}\,\Psi_{pq}(r)\,\omega_p(\theta) \qquad (28)$$

The solution of equation (26) is written in the form

$$p = \sum_{p=0}^{\infty}\sum_{q=1}^{\infty} a_{pq}\,P_{pq}(z)\,\Psi_{pq}(r)\,\omega_p(\theta) \qquad (29)$$

(*) See footnote to equation (16).

** The validity of the expansion depends on the existence of Green's function for the boundary condition $\frac{\partial p}{\partial r}(b) = 0$, which follows from the existence of Green's function for the boundary condition $p(1) = 0$. (12, 13)

The transverse eigenfunctions must satisfy the relation stated previously in equation (21). Then equation (26) yields

$$a_{pq}\left[\frac{d^2 R_{pq}}{dz^2} - (s^2 + s_{pq}^2) R_{pq}\right] = A_{pq} F(z) \qquad \text{for all } p, q$$

Let $a_{pq} = A_{pq}$. Thus, the partial differential equation (26) has been reduced to the set of linear, second order, inhomogeneous, ordinary differential equations.

$$\frac{d^2 R_{pq}}{dz^2} - (s^2 + s_{pq}^2) R_{pq} = F(z) \qquad (30)$$

The expansion coefficients are given by

$$A_{pq} = \frac{1}{H} \int_{\theta=0}^{2\pi} \int_{r=0}^{1} G(r,\theta) \Psi_{pq} \Theta_p^* \, r \, dr \, d\theta \qquad (31)$$

where H is a normalizing factor, defined by

$$H = \int_0^{2\pi} \int_0^1 \Psi_{pq}^2 \Theta_p \Theta_p^* \, r \, dr \, d\theta \qquad (32)$$

and Θ_p^* is the complex conjugate of Θ_p

Consider first the partial solution ψ_B, given by

$$\psi_B = \sum_{p=0}^{\infty} \sum_{q=0}^{\infty} B_{pq} R_{B_{pq}}(z) \Psi_{pq}(r) \Theta_p(\theta) \qquad (33)$$

where the axial distribution functions $R_{B_{pq}}$ satisfy the differential equations(*)

$$\frac{d^2}{dz^2}\left(\frac{R_{B_{pq}}}{R_{00}}\right) - (s^2 + s_{pq}^2)\left(\frac{R_{B_{pq}}}{R_{00}}\right) = \mathcal{R} \frac{d\bar{u}}{dz} \qquad (34)$$

The mode of instability under consideration is specified by the pair of indices ν, h. If p = ν, q = h, equation (34) reduces to

$$\frac{d^2}{dz^2}\left(\frac{R_{B_{\nu h}}}{R_{00}}\right) = \mathcal{R} \frac{d\bar{u}}{dz} \qquad (35)$$

(*) Here, it is assumed that ℓ_r, and hence $\mathcal{R}$, do not depend on r or θ. The opposite case can easily be treated.

exactly as for the partial solutions p_A and p_D. Then

$$\frac{p_{\beta\nu h}}{p_\infty} = R\int_0^z \bar{u}(z')dz' + K_{\beta\nu h} \tag{36}$$

as before. For all other values of p and q, equation (34) becomes

$$\frac{d^2}{dz^2}\left(\frac{p_{\beta pq}}{p_\infty}\right) - (s_{pq}^2 - s_{\nu h}^2)\left(\frac{p_{\beta pq}}{p_\infty}\right) = R\frac{d\bar{u}}{dz} \tag{37}$$

since $s^2 = -s_{\nu h}^2 + O(a_e)$. The solution of this equation is obtained by the method of variation of constants as

$$\frac{p_{\beta pq}}{p_\infty} = R\int_0^z \frac{d\bar{u}}{dz}(z')\frac{\sinh\sqrt{s_{pq}^2 - s_{\nu h}^2}(z-z')}{\sqrt{s_{pq}^2 - s_{\nu h}^2}}dz' + K_{\beta pq}\cosh\sqrt{s_{pq}^2 - s_{\nu h}^2}\,z \tag{38}$$

The expansion coefficients B_{pq} are given by

$$B_{pq} = \frac{\int_0^{2\pi}\int_0^1 \frac{d\Psi_{\nu h}}{dr}\Psi_{pq}\omega_\nu\omega_p^* r\,dr\,d\theta}{\int_0^{2\pi}\int_0^1 \Psi_{pq}^2\omega_p\omega_p^* r\,dr\,d\theta} \tag{39}$$

For a spinning mode, $\omega_p = e^{-ip\theta}$. Then

$$B_{pq} = \frac{\int_0^{2\pi} e^{-i\nu\theta}e^{ip\theta}d\theta\int_0^1 s_{\nu h}\frac{dJ_\nu}{dr}(s_{\nu h}r)J_p(s_{pq}r)\,r\,dr}{\int_0^{2\pi}d\theta\int_0^1 J_p^2(s_{pq}r)\,r\,dr} \tag{40}$$

From this expression, since the function $e^{-i\nu\theta}$ and $e^{ip\theta}$ are orthogonal, it can be seen that*

$$B_{pq} = 0, \quad p \neq \nu \tag{41}$$

$$B_{\nu q} = \frac{s_{\nu q}\int_0^1 J_\nu'(s_{\nu h}r)J_\nu(s_{\nu q}r)\,r\,dr}{\int_0^1 J_\nu^2(s_{\nu q}r)\,r\,dr}$$

---

* A prime will be used to denote differentiation of a function with respect to its argument. Thus $J_\nu'(x) = \frac{dJ_\nu}{dx}$

The same result is obtained for the standing mode, because $\cos \nu\theta$ and $\cos p\theta$ ($0 \leq \theta \leq 2\pi$) are also orthogonal.

The partial solution p_C is obtained by the same procedure as used for p_B. Thus, letting

$$p_C = \sum_{p=0}^{\infty} \sum_{q=1}^{\infty} C_{pq} P_{cpq}(z) \Psi_{pq}(r) \Phi_p(\theta), \tag{42}$$

the axial distribution functions are(**)

$$\frac{P_{c\nu h}}{P_{oo}} = \mathcal{J} \int_0^z \bar{u}(z')\, dz' + K_{c\nu h} \tag{43a}$$

$$\frac{P_{opq}}{P_{oo}} = \mathcal{J} \int_0^z \frac{d\bar{u}}{dz}(z') \frac{\sinh \sqrt{s_{pq}^2 - s_{\nu h}^2}\,(z - z')}{\sqrt{s_{pq}^2 - s_{\nu h}^2}}\, dz' + K_{pq} \cosh \sqrt{s_{pq}^2 - s_{\nu h}^2}\, z \tag{43b}$$

The expansion coefficients for p_C are given by the expression

$$C_{pq} = \frac{\int_0^1 \int_0^{2\pi} \frac{1}{r} \Psi_{\nu h}(r) \Psi_{pq}(r) \Phi_\nu'(\theta) \Phi_p^*(\theta)\, r\, dr\, d\theta}{\int_0^1 \int_0^{2\pi} \Psi_{pq}^2 \Phi_p(\theta) \Phi_p^*(\theta)\, r\, dr\, d\theta} \tag{44}$$

For a spinning mode $\Phi_\nu = e^{i\nu\theta}$. Then $\Phi_\nu' = -i\nu e^{-i\nu\theta}$ is orthogonal to all of the functions $\Phi_p^+ = e^{ip\theta}$ except Φ_ν^+, so that

$$C_{pq} = 0 \quad \text{for} \quad p \neq \nu \tag{45a}$$

and

$$C_{\nu q} = -i\nu \frac{\int_0^1 J_\nu(s_{\nu h} r) J_\nu(s_{\nu q} r)\, dr}{\int_0^1 J_\nu^2(s_{\nu q} r)\, r\, dr} \tag{45b}$$

** The assumption is made here that ℓ_o, and r, do not depend on r or θ. It is easy to treat the opposite case.

In particular, for q = h, equations (45b) becomes

$$C_{\nu h} = -i\nu \frac{\int_0^1 J_\nu^2(s_{\nu h} r)\, dr}{\int_0^1 J_\nu^2(s_{\nu h} r)\, r\, dr} = -i\,\tilde{C}_{\nu h} \qquad (46)$$

where $\tilde{C}_{\nu h}$ is a positive real number. Thus, the expansion coefficient corresponding to the mode of instability under consideration is a negative, purely imaginary number.

However, for a standing mode of oscillation, $\Phi_\nu = \cos\nu\theta$, and the derivative $\Phi_\nu' = -\nu \sin\nu\theta$ is orthogonal to $\Phi_p^* = \cos p\theta$ for all p, over the interval $0 \le \theta \le 2\pi$. In order to obtain expressions for the expansion coefficients, the interval of definition of the eigenfunction expansion is changed from $0 \le \theta \le 2\pi$ to $0 \le \theta \le \pi$. Since the standing mode oscillation pattern is symmetrical about $\theta = 0 \ (\text{or } \theta = \pi)$, the other half of the solution can be obtained by reflection. Then for a standing mode,

$$C_{pq} = -\nu \frac{\int_0^\pi \sin\nu\theta \cos p\theta\, d\theta \int_0^1 J_\nu(s_{\nu h} r) J_p(s_{pq} r)\, dr}{\int_0^\pi \cos^2 p\theta\, d\theta \int_0^1 J_p^2(s_{pq} r)\, r\, dr}$$

or

$$C_{pq} = 0 \quad \text{for } p - \nu = 2m, \ m = 0, \pm 1, \pm 2, \cdots$$

$$C_{pq} = -\frac{4\nu^2}{\pi(p^2 - \nu^2)} \frac{\int_0^1 J_\nu(s_{\nu h} r) J_p(s_{pq} r)\, dr}{\int_0^1 J_p^2(s_{pq} r)\, r\, dr} \qquad (47)$$

$$\text{for } p - \nu = 2m + 1, \ m = 0, \pm 1, \pm 2, \cdots$$

The most important result here is that the eigenfunction expansion for p_c does not include a term corresponding to the mode of which the stability is being considered.

In summary, the solution for the pressure perturbation has been found to be

$$p' = \left\{ \left[P_0(z) + P_A(z) + B_{\nu h} P_{B\nu h}(z) - i C_{\nu h} P_{C\nu h}(z) + P_D(z) \right] J_\nu(s_{\nu h} r) \right. \tag{48}$$

$$\left. + \sum_{q \neq h} \left[B_{\nu q} P_{B\nu q}(z) + C_{\nu q} P_{C\nu q}(z) \right] J_\nu(s_{\nu q} r) \right\} e^{-i\nu\theta}$$

for the spinning mode, and

$$p' = \left\{ \left[P_0(z) + P_A(z) + B_{\nu h} P_{B\nu h}(z) + P_D(z) \right] J_\nu(s_{\nu h} r) \right.$$

$$\left. + \sum_{q \neq h} B_{\nu q} P_{B\nu q}(z) J_\nu(s_{\nu q} r) \right\} \cos \nu\theta \tag{48b}$$

$$+ \sum_{\substack{p-\nu \\ \text{odd}}} \sum_{q} C_{pq} J_p(s_{pq} r) \cos p\theta$$

for the standing mode. Both of these solutions are of the form

$$p' = \left[P_0(z) + P_{1\nu h}(z) \right] \Psi_{\nu h}(r) \Theta_\nu(\theta) + \sum_{p} \sum_{q \neq \nu, h} P_{1pq}(z) \Psi_{pq}(r) \Theta_p(\theta) \tag{49a}$$

so that the velocity perturbations can be written as

$$u' = -\frac{1}{\gamma s} \left[\left(\frac{dP_0}{dz} + \frac{dP_{1\nu h}}{dz} \right) \Psi_{\nu h} \Theta_\nu + \sum_{p} \sum_{q} \frac{dP_{1pq}}{dz} \Psi_{pq} \Theta_p \right] \tag{49b}$$

$$v' = -\frac{1}{\gamma s} \left\{ \left[\left(1 + \frac{k' \bar{\rho}_1}{s} + \frac{1}{s} \frac{d\bar{u}}{dz} \right) P_0 + P_{1\nu h} \right] \Psi'_{\nu h} \Theta_\nu + \sum_{p} \sum_{q} P_{1pq} \Psi'_{pq} \Theta_p \right\} \tag{49c}$$

$$w' = \frac{1}{\gamma s} \left\{ \left[\left(1 + \frac{k' \bar{\rho}_1}{s} + \frac{1}{s} \frac{d\bar{u}}{dz} \right) P_0 + P_{1\nu h} \right] \frac{\Psi_{\nu h}}{r} \Theta'_\nu + \sum_{p} \sum_{q} P_{1pq} \frac{\Psi_{pq}}{r} \Theta'_p \right\} \tag{49d}$$

The entropy perturbation must be evaluated before the nozzle boundary condition can be imposed. As with the other perturbation quantities, the entropy is written as

$$s' = s_0 + s_1 + \cdots \tag{50}$$

where it is found that

$$\begin{aligned} s_0 &= 0 \\ s_1 &= -\frac{1}{S}\frac{d\bar{u}}{dz}\left(\frac{\gamma-1}{\gamma}\right)p_0 \end{aligned} \tag{51}$$

Thus the entropy perturbation is largest in the region where the combustion is most intense. At the nozzle entrance, where combustion is assumed complete, the entropy perturbation vanishes to $O(\bar{u}_e)$.

It is now possible to examine the stability behavior of the rocket motor by applying the chamber exit boundary condition, which is the nozzle admittance relation. The conditions at the stability limits, which bound the regions of unstable operation, will be derived by setting the amplification factor λ equal to zero. Then the complex time parameter s is purely imaginary, $s = i\omega$, where ω is the frequency of oscillation.

The boundary condition imposed by the exhaust nozzle upon the oscillatory flow in the rocket combustion chamber was presented in Reference 1 as

$$\frac{\gamma u_e}{p_0} + A\frac{p_e}{p_0} + B S_{sh}\frac{\gamma V_e}{p_0} + e\frac{\gamma S_e}{p_0} = 0 \tag{52}$$

In this form it is applicable to the case in which the combustion process is sensitive only to pressure variations. However, because of the distortion of the wave pattern introduced by the effects on the combustion process of the transverse velocity fluctuations, it has been necessary in here to make use of

eigenfunction expansions in the perturbation solution, which has been found to take the following form:

$$
\begin{aligned}
p' &= \sum_p \sum_g P_{pg}(z)\,\Psi_{pg}(r)\,\Theta_p(\theta) \\
u' &= \sum_p \sum_g U_{pg}(z)\,\Psi_{pg}(r)\,\Theta_p(\theta) \\
v' &= \sum_p \sum_g V_{pg}(z)\,\Psi_{pg}(r)\,\Theta_p(\theta) \\
w' &= \sum_p \sum_g V_{pg}(z)\,\frac{1}{r}\,\Psi_{pg}(r)\,\Theta'_p(\theta) \\
s' &= \sum_p \sum_g S_{pg}(z)\,\Psi_{pg}(r)\,\Theta_p(\theta)
\end{aligned}
\qquad (53)
$$

Then, imposing the nozzle boundary condition results in not one relation as in equation (52), but infinitely many relations of the form

$$
\frac{\gamma U_{pg}(z_e)}{P_{oo}} + A\,\frac{P_{pg}(z_e)}{P_{oo}} + B_{spg}\,\frac{\gamma V_{pg}(z_e)}{P_{oo}} + C\,\frac{\gamma S_{pg}(z_e)}{P_{oo}} = 0 \qquad (54)
$$

There is thus an admittance relation corresponding to each term in the eigenfunction expansions.

Since combustion is assumed to be complete at the entrance to the nozzle,

$$
\frac{d\bar{u}}{dz}(z=z_e) = \bar{P}_z(z=z_e) = 0
$$

Hence, the axial distribution functions become, using equations (48) and (49a)

$$
\begin{aligned}
P_{\nu h}(z_e) &= P_o(z_e) + P_A(z_e) + B_{\nu h} P_{o\nu h}(z_e) - i C_{\nu h} P_{c\nu h}(z_e) + P_D(z_e) \\
P_{pg}(z_e) &= B_{pg} P_{opg}(z_e) + C_{pg} P_{cpg}(z_e) \\
U_{pg}(z_e) &= -\frac{1}{\gamma s}\,\frac{dP_{pg}}{dz}(z_e) \\
V_{pg}(z_e) &= -\frac{1}{\gamma s}\,P_{pg}(z_e) \\
S_{pg}(z_e) &= 0
\end{aligned}
\qquad (55)
$$

where

$$P_0(z) = P_{00}\left[1 + (s^2 + s_{\nu h}^2)\frac{z^2}{2}\right]$$

$$P_A(z) = P_{00}\left[-\gamma s \mathcal{P}\int_0^z \bar{u}\,dz' + K_A\right] \qquad (56)$$

$$P_{B\nu h}(z) = P_{00}\left[\mathcal{R}\int_0^z \bar{a}\,dz' + K_{B\nu h}\right]$$

$$P_{C\nu h}(z) = P_{00}\left[\mathcal{J}\int_0^z \bar{u}\,dz' + K_{C\nu h}\right]$$

$$P_D(z) = P_{00}\left[s\int_0^z dz'\int_0^{z'} k'\bar{\rho}_2\,dz'' + (\gamma+1)s\int_0^z \bar{u}\,dz' + K_D\right]$$

$$P_{Bpq}(z) = P_{00}\left[\mathcal{R}\int_0^z \frac{d\bar{u}}{dz}\,\frac{\sinh\gamma\sqrt{s_{pq}^2 - s_{\nu h}^2}\,(z-z')}{\gamma\sqrt{s_{pq}^2 - s_{\nu h}^2}}\,dz' + K_{Bpq}\cosh\gamma\sqrt{s_{pq}^2 - s_{\nu h}^2}\,z\right]$$

$$P_{Cpq}(z) = P_{00}\left[\mathcal{J}\int_0^z \frac{d\bar{u}}{dz}\,\frac{\sinh\gamma\sqrt{s_{pq}^2 - s_{\nu h}^2}\,(z-z')}{\gamma\sqrt{s_{pq}^2 - s_{\nu h}^2}}\,dz' + K_{pq}\cosh\gamma\sqrt{s_{pq}^2 - s_{\nu h}^2}\,z\right]$$

Substituting the relations (55) into the nozzle admittance equation (54), and defining a combined admittance coefficient $\mathcal{E}$ by

$$\mathcal{E} = \mathcal{E}_r + i\,\mathcal{E}_i = A\left(\frac{\omega}{s_{pq}}\right) + i\,B \qquad (57)$$

there results the equation

$$\left(\frac{d}{dz} - i\,s_{pq}\mathcal{E}\right)\frac{P_{pq}}{P_{00}}(z_e) = 0 \qquad (58)$$

Each of the partial solutions making up the pressure perturbation p' includes a constant resulting from the integration in the axial direction. For each pair of indices p, q (that is, for each term in the eigenfunction expansion), the several integration constants can be combined into one. Then the axial distribution functions $P_{pq}(z)$ take the following form:

$$P_{pq}(z) = P_{00}\left[\tilde{P}_{pq}(z) + K_{pq}\cos\gamma\sqrt{s_{pq}^2 - s_{\nu h}^2}\,z\right] \qquad (59)$$

where the function $\tilde{P}_{pg}$ does not include any integration constant and the constants K_{pg} are all $O(\bar{u}_e)$. In particular, the axial function corresponding to the mode of oscillation under consideration can be written as

$$P_{\nu h}(z) = P_{00}\left[1 + K_{\nu h} + \tilde{P}_{1\nu h}(z)\right] \tag{60}$$

The function $\tilde{P}_{1\nu h}$, which from equations (55) and (56) is given by

$$\tilde{P}_{1\nu h}(z) = (\delta^2 + s_{\nu h}^2)\frac{z^2}{2} + s\int_0^z dz' \int_0^{z'} k'\bar{\rho}_e\, dz'' + \left[(\gamma+1)s - \gamma_s P + \beta_{\nu h} R - i\mathcal{C}_{\nu h} J\right]\int_0^z \bar{u}\, dz, \tag{61}$$

is $O(\bar{u}_e)$. The integration constant $K_{\nu h}$ can be absorbed into the constant P_{00} as can be seen from the following discussion. Equation (59) is divided through by $\tilde{P}_{00} = P_{00}(1 + K_{\nu h})$, giving

$$\frac{P_{\nu h}}{\tilde{P}_{00}} = 1 + \frac{\tilde{P}_{1\nu h}}{1 + K_{\nu h}} = 1 + \tilde{P}_{1\nu h}(1 - K_{\nu h}) + O(\bar{u}_e^3)$$

or

$$\frac{P_{\nu h}}{P_{00}} = 1 + \tilde{P}_{1\nu h} - K_{\nu h}\tilde{P}_{1\nu h} + O(\bar{u}_e^3)$$

Since both $K_{\nu h}$ and $\tilde{P}_{1\nu h} = O(\bar{u}_e)$, their product is $O(\bar{u}_e^2)$, and thus

$$P_{\nu h}(z) = \tilde{P}_{00}\left(1 + \tilde{P}_{1\nu h}\right) + O(\bar{u}_e^2) \tag{62}$$

Similarly, replacing P_{00} with $\tilde{P}_{00}$ in equation (59) results in an error of $O(\bar{u}_e^2)$ which in this analysis has been assumed to be negligible.

The solution for the pressure perturbation, equation (49a), can thus be written

$$P'(z,r,\theta) = \tilde{P}_{00}\left\{\left[1 + \tilde{P}_{1\nu h}(z)\right]\Psi_{\nu h}(r)\Theta_{\nu}(\theta) + \sum_{p,g\neq\nu,h}\sum\left[\tilde{P}_{pg}(z) + K_{pg}\cosh\sqrt{s_{pg}^2 - s_{\nu h}^2}\,z\right]\Psi_{pg}(r)\Theta_p(\theta)\right\} \tag{63}$$

The constant $\tilde{P}_{oo}$, which represents the perturbation amplitude level, will not affect the stability solution. For each $p, q \neq y, h$ the nozzle boundary condition

$$\frac{d\tilde{P}_{pq}}{dz}(z_e) + K_{pq}\sqrt{s_{pq}^2 - s_{vh}^2}\sinh\sqrt{s_{pq}^2 - s_{vh}^2}\,z_e \qquad (64a)$$

$$-i s_{pq}\,\varepsilon(\omega, s_{pq})\left[\tilde{P}_{pq}(z_e) + K_{pq}\cosh\sqrt{s_{pq}^2 - s_{vh}^2}\,z_e\right] = 0$$

can be used to determine the integration constant K_{pq}. Application of the remaining boundary condition,

$$\frac{d\tilde{P}_{vh}}{dz}(z_e) - i s_{vh}\,\varepsilon(\omega, s_{vh})\left[1 + \tilde{P}_{1vh}(z_e)\right] = 0 \qquad (64b)$$

results in an eigenvalue problem. That is, equation (64b) is the characteristic equation for the eigenvalues s, or $i\omega$, since as already stated we are only concerned with the stability limits where $\lambda = 0$.

By use of the expression for $P_{vh}(z)$ obtained from equations (60) and (61), the characteristic equation (64b) can be written as

$$P + i\left(\frac{\beta_{vh}}{\gamma\omega}\right)R + \left(\frac{\tilde{\omega}_{vh}}{\gamma\omega}\right)J = h \qquad (65)$$

where the right hand side is of the form

$$h = \frac{\gamma+1}{\gamma} + \frac{h_2}{h_1}$$

with

$$h_1 = \gamma\bar{u}_e - i\gamma s_{vh}\,\varepsilon\int_0^{z_e}\bar{u}(z)\,dz \qquad (66a)$$

$$h_2 = \int_0^{z_e} k'(z)\bar{P}_1(z)\,dz + i s_{vh} z_e\left(f - \frac{1}{f}\right)$$

$$-\varepsilon\left[\frac{1}{f} - \frac{s_{vh}^2 z_e^2}{2}\left(f - \frac{1}{f}\right) + i s_{vh}\int_0^{z_e} dz \int_0^{z} k'(z')\bar{P}_1(z')\,dz'\right] \qquad (66b)$$

In the expressions for h_1 and h_2 a reduced frequency $f = \frac{\omega}{s_{vh}}$ has been introduced. Since $\omega^2 - s_{vh}^2 = O(\bar{u}_e)$ for a purely transverse mode, the reduced frequency f takes on values near unity.

As written in equation (65) above, the characteristic equation exhibits the balance which exists at the stability limits. In order for neutral oscillations to be maintained, the energy supplied by the combustion process, related to the left side of equation (65), must be completely absorbed by the fluid mechanical processes, which are related to the function h on the right side of the characteristic equation. If more than sufficient energy is supplied, the oscillation amplitude will grow. Such an oscillation is linearly unstable. Eventually, nonlinear energy-absorbing processes will restore the energy balance at some high level of amplitude. The importance of the oscillation to the proper operation of the rocket motor depends upon the amplitude level finally attained. However, it has been observed that nearly all transverse mode instabilities grow to very high levels, causing rapid combustion chamber destruction. Stable operation results in the case that the energy release is insufficient to balance the energy absorbed by the oscillation. The fact that the characteristic equation is complex implies that there is a phase condition, as well as the amplitude condition, relating the oscillating rates of energy release and energy absorption for neutral oscillations.

Assuming first that the pressures and velocity effects are characterized by the same mean sensitive time lag τ, the definitions of the burning rate parameters are obtained from (12a) as

$$\begin{aligned} P &= n\left(1 - e^{-i\omega\tau}\right) \\ R &= l_r\left(1 - e^{-i\omega\tau}\right) \\ J &= l_e\left(1 - e^{-i\omega\tau}\right) \end{aligned} \tag{68}$$

The simplification of these expressions with respect to (12a) can be justified (3) and corresponds to neglecting the space wise contributions to the burning rate oscillation. Then the characteristic equation takes the form

$$\left[1+ i\left(\frac{B_{vh}}{\gamma\omega}\right)\frac{l_r}{n} + \left(\frac{\tilde{\zeta}_{vh}}{\gamma\omega}\right)\frac{l_0}{n}\right] n\left(1-e^{-i\omega\tau}\right) = h(\omega) \qquad (69)$$

This complex equation is equivalent to two real equations. Therefore, for neutral oscillations of a given rocket motor, the four combustion parameters, n, τ, $\frac{l_r}{n}$ and $\frac{l_0}{n}$, are not independent. If any three are known, then the fourth, together with the oscillation frequency, can be determined from equation (69). Because the frequency dependence of $h(\omega)$ is quite complicated, it is most convenient to regard the frequency as one of the independent variables. In order that the present investigation may be related more easily to previous studies of both longitudinal and transverse modes, the two dependent variables will be taken to be the mean sensitive time lag τ and the pressure interaction index n. Thus,

$$n = n\left(\omega, \frac{l_r}{n}, \frac{l_0}{n}\right)$$

$$\tau = \tau\left(\omega, \frac{l_r}{n}, \frac{l_0}{n}\right)$$

will be determined from the characteristic equation, which can be written as

$$n\left(1-e^{-i\omega\tau}\right) = \frac{h}{1+i\frac{B_{vh}}{\gamma\omega}\frac{l_r}{n}+\frac{\tilde{\zeta}_{vh}}{\gamma\omega}\frac{l_0}{n}} = \tilde{h} = \tilde{h}_r + i\tilde{h}_i \qquad (70)$$

clearly, if only pressure effects are present, $\tilde{h} = h$.

At present, none of the combustion parameters can be calculated <u>a priori</u>, although a method has been developed for measuring n and τ experimentally (4). Since very little is quantitatively known about the velocity parameters, their

effects will be shown by calculating n and τ for assumed values of the ratios $\frac{l_r}{h}$ and $\frac{l_\theta}{h}$. The modifications introduced by the assumed velocity effects will then be noted and compared with the results of appropriate experiments.

The real and imaginary parts of equation (70),

$$n(1-\cos\omega\tau) = \tilde{h}_r$$
$$n\sin\omega\tau = \tilde{h}_i \qquad (71)$$

comprise a dimultaneous pair of equations for n and τ. The solution is found to be

$$n = \frac{\tilde{h}_r^2 + \tilde{h}_i^2}{2\tilde{h}_r} \qquad (72)$$
$$\tau = \frac{1}{\omega}\sin^{-1}\left(\frac{\tilde{h}_i}{n}\right) = \frac{1}{\omega}\cos^{-1}\left(1-\frac{\tilde{h}_r}{n}\right)$$

where τ is determined modulo $\frac{2\pi}{\omega}$.

A typical solution for $n(\omega)$ and $\tau(\omega)$ for assumed values of $\frac{l_r}{h}$ and $\frac{l_\theta}{h}$ is shown in Figure 5. This solution applies at the stability limits, where $\lambda = 0$. It can be seen that for any given value of the time lag, only one value of the pressure interaction index is consistent with neutral oscillations. For the same τ, a larger value of n corresponds to instability $(\lambda>0)$, a smaller value to stability $(\lambda<0)$. Thus the n,τ plane is divided by the loci of $\lambda = 0$ into stable and unstable regions, as shown in Figure 6.

A given rocket motor system at given operating conditions is assumed to be characterized by a set of values of the combustion parameters n,τ, $\frac{l_r}{h}$ and $\frac{l_\theta}{h}$. If the point on the n,τ -plane representing this motor falls within one of the unstable regions (i.e., above the stability limit curve) corresponding to one of the transverse modes and to the appropriate

values of $\frac{l_r}{n}$ and l_{θ}/n, then the operation of the rocket will be unstable, and large amplitude oscillations can be expected to result. Therefore, any effect which increases the size of the unstable areas on the n,τ-plane (e.g., by shifting the stability limits to smaller n for all τ, or by flattening the limit curves without changing n_m) is a destabilizing effect.

In order to clarify the discussion, the effects of tangential and radial velocity fluctuations will be considered separately. First, suppose that only pressure and tangential velocity oscillations affect the combustion process rates (corresponding to a tangentially oriented doublet injector pattern). Then the characteristic equation can be written

$$n\left(1-e^{-i\omega\tau}\right)=\tilde{h}=\frac{h}{1+\frac{\tilde{c}_{vh}}{r\omega}\frac{l_\theta}{n}} \tag{73}$$

For real values of l_{θ}/n, the ratio $\tilde{h}/h$ is real-valued, and there is no shift of the stability limit curve in the τ-direction. The ratio of the minimum interaction index including tangential velocity effects, n_{mT}, to that for pressure effects alone, n_{mp}, is

$$\frac{n_{mT}}{n_{mp}}=\frac{\tilde{h}}{h}=\frac{1}{1+\frac{\tilde{c}_{vh}}{r\omega}\frac{l_\theta}{n}} \tag{74}$$

Therefore, since $\frac{\tilde{c}_{vh}}{r\omega}>0$, a positive value of the tangential velocity index causes a downward shift of the stability limit curve on the n,τ plane by contracting the ordinates of the limit points, which is a destabilizing trend. Figure 7a shows the influence of the tangential velocity effect on the stability limits for the first tangential spinning mode. For other modes of

oscillation, the effects will be qualitatively the same. The magnitude of the velocity effect, for a given $\frac{l_\theta}{n}$ value, depends on the ratio of the expansion coefficient $\tilde{\zeta}_{\nu h}$ to the frequency $\omega = f s_{\nu h}$. This ratio is approximately equal to $\frac{\tilde{\zeta}_{\nu h}}{s_{\nu h}}$, values of which are given in Table I for several modes. The second tangential mode is seen to be slightly more influenced by the tangential velocity oscillations than the other modes. It should be recalled that the expansion coefficient $\tilde{\zeta}_{\nu h}$ vanishes for a standing tangential mode, so that there are no tangential velocity effects for such an oscillation.*

The velocity index l_θ is positive in the case that the burning rate is increased by a positive velocity. For the tangential velocity, the positive direction is not fixed with respect to the rocket combustion chamber, but is the direction in which a spinning wave travels.** Assuming that the injector is characterized by a positive l_θ direction (determined by the orientation of the injection pattern), the velocity effect of a wave moving in the positive direction will augment the pressure effect. However, for a wave moving in the other direction, the velocity effect will oppose that of the pressure. It is apparent, therefore, that the preferred wave travel direction with respect to the physical frame of reference is the same as the positive l_θ direction of the injector.

If the tangential velocity effects are in reality a result of a tangential displacement sensibility, the value of m_θ is real and, as (9c) shows,

---

* However, this may not be true if l_θ changes periodically with θ.

** See footnote to equation (16).

ℓ_θ must be imaginary. In Figure 7b the results relative to the case $\ell_\theta/n = i$ * are compared with those of $\ell_\theta/n = 0$ and 1, showing that the tangential displacement effect, contrary to the tangential velocity effect, produces larger changes in the value of τ then in those of n. Also shown in the figure is the case when both effects are simultaneously present, characterized by $\ell_\theta/n = 1+i$.

Consider now the effect of the radial velocity coupled with the pressure, i.e., $\ell_r \neq 0$ but $\ell_\theta = 0$. Then the characteristic equation is

$$n(1-e^{-i\omega\tau}) = \tilde{h} = \frac{h}{1+i\frac{B_{vh}}{\tau\omega}\frac{\ell_r}{n}} \tag{75}$$

Since the ratio $\tilde{h}/h$ is complex, one can expect an influence on τ as well as on n. As shown in Figure 8a, for a positive radial velocity index ℓ_r, the limit curve is shifted in the direction of longer time lags. In the cylindrical coordinate system, the positive radial direction is from the center of the chamber toward the outer wall. If a positive velocity increases the burning rate, ℓ_r is positive and the stability limit curve is shifted toward longer τ, and vice versa. However, it can be seen that the magnitude of the radial velocity effect is much smaller than that of the tangential velocity for equal velocity interaction indices.

Figure 8b shows the effects of radial displacement sensitivity. This time the main effect is a shift of n, while it was a shift of τ for the radial velocity effect. It is clear that a positive radial displacement sensitivity ($\ell_r/n = -i$, $m_r/n = \omega$) is stabilizing, and a negative sensitivity

---

* This value is independent of the frequency, which means that m_θ should depend on it, according to (9c).

($\ell_r/n = i$, $m_r/n = -\omega$) is destabilizing.

In order to check to what extent this result depends on the existence of a time lag, we consider now the case when instanteous effects are the only ones to be present, that is P = 0 and $\mathcal{R}$ and $\mathcal{T}$ given by equations (12b). Equation (65) becomes

$$\frac{B_{vh}}{\gamma\omega^2} m_r - i \frac{\tilde{C}_{vh}}{\gamma\omega^2} m_\theta = h \qquad (76)$$

Calculating for simplicity the case $k' = 0$ (negligible droplet drag effects), we obtain, using equations (66a and b) and separating real from imaginary,

$$\left(\frac{B_{vh}}{\omega^2} m_r - \gamma - 1\right)\left(\bar{u}_e + s_{vh}\varepsilon_i \int_0^{z_e} \bar{u}\,dr\right) - \frac{\tilde{C}_{vh}}{\omega^2} m_\theta s_{vh}\varepsilon_r \int_0^{z_e} \bar{u}\,dr = -\varepsilon_r\left[\frac{1}{f} - \frac{s_{vh}^2 z_e^2}{2}\left(f - \frac{1}{f}\right)\right]$$

$$\left(\frac{B_{vh}}{\omega^2} m_r - \gamma - 1\right) s_{vh}\varepsilon_r \int_0^{z_e} \bar{u}\,dr + \frac{\tilde{C}_{vh}}{\omega^2} m_\theta\left(\bar{u}_e + s_{vh}\varepsilon_i \int_0^{z_e} \bar{u}\,dr\right) = \varepsilon_i\left[\frac{1}{f} - \frac{s_{vh}^2 z_e^2}{2}\left(f - \frac{1}{f}\right)\right]$$

Let us first consider the case $m_\theta = 0$. If m_r is eliminated from the resulting equations one gets an equation in which the only unknown is f or ω (of which ε_r and ε_i are also functions). The solution of this equation for any given mode provides the deviation of the frequency at the stability limits from the corresponding acoustic frequency. It can easily be checked deviation is rather small, and f is close to 1. Once the frequency is determined any of the original equations can be used to determine m_r, for instance

$$\frac{B_{vh}}{\omega^2} m_r = \gamma + 1 - \frac{\varepsilon_r\left[\frac{1}{f} - \frac{s_{vh}^2 z_e^2}{2}\left(f - \frac{1}{f}\right)\right]}{\bar{u}_e + s_{vh}\varepsilon_i \int_0^{z_e} \bar{u}\,dr} \qquad (77)$$

$$\cong \gamma + 1 - \frac{\varepsilon_r}{\bar{u}_e}$$

the test simplification being allowed by the fact that $f \cong 1$ and the second term in the denominator is substantially smaller than the first. Numerical examples shows that generally the second member of equation (77) is positive. Hence, since for tangential modes $B_{vh} > 0$, a positive value of m_r is required to produce neutral oscillations. It is easily seen that a value larger than this positive value would result in unstable behavior. Clearly, if pressure effects were present too, we would find the same result obtained previously, namely . that a positive value of m_r is destabilizing. This result, which holds for both spinning and standing tangential modes, shows the importance of designing the injector in such a way that the more volatile propellant droplets are not systematically located at a smaller radius than the partner propellant. Observe that the opposite conclusion is reached for the first radial mode which has a negative B_{vh}. This, however, occurs at a substantially higher frequency.

Similarly if $m_r = 0$ one obtains

$$\frac{\tilde{C}_{vh}}{\omega^2} m_\theta = \frac{\frac{1}{f} - \frac{\Lambda_{vh}^2 z_e^2}{8}\left(f - \frac{1}{f}\right)}{\Lambda_{vh} \int_0^{z_e} \bar{u}\, dr} \cong \frac{1}{\Lambda_{vh} \int_0^{z_e} \bar{u}\, dr}$$

Again, for positive $\tilde{C}_{vh}$, as happens to be the case for spinning modes, values of m_θ in excess of a definite positive value produce instability. For standing modes $\tilde{C}_{vh}$ matches identically and no instability can result from this mechanism.

One must recall here that the above results are obtained for m_r, l_r and m_θ, l_θ independent of r and θ, that is, for a uniform injector pattern. If m_θ or l_θ were made to change periodically with θ the conclusions concerning spinning and standing modes might be reversed. Similarly if m_r or l_r is a function of r the above conclusion concerning the radial modes might be changed.

Observe also that while a uniformly positive m_r or l_r can be detected in many injector designs, a uniformly positive m_θ or l_θ is generally not found (except in experimental conditions where it is so designed) because of a tendency of designers toward symmetric designs.

IV. EXPERIMENTAL VERIFICATION

From the linearized velocity sensitivity theory the result is obtained that the tangential velocity effects are absent in standing modes and present in spinning modes. The tangential velocity perturbation acts to shift the stability limits on the n,τ -plane to smaller values of the interaction index. The effect of the radial velocity perturbation is to shift the stability limits to larger or smaller time lag values, depending on the sign of the velocity index. A positive velocity index is associated with the tangential velocity effect. However, the positive tangential direction is not defined in terms of the combustion chamber geometry, as in the case of the radial velocity. Rather, the positive tangential direction is defined as the direction in which a spinning wave travels.

The sign of the velocity index depends on the characteristics of the spray formed by the injector. According to the physical model, a positive velocity index implies that the burning rate is increased when the velocity perturbation is in the positive direction. The symmetry of the fuel-on-oxidizer impinging doublet injector is such that the radial and tangential velocity effects can be separated, as discussed previously. For the radial spud orientation (see Figure 2), the velocity effect, due solely to the radial velocity component, cannot be calculated unless the sign of the velocity index is known for a particular injector arrangement. At the present time, knowledge of the details of the combustion process is insufficient to allow the prediction of the velocity index sign. Therefore, one must resort to ex-

perimental means, based on spinning mode tests with the tangential spud orientation. By observing the direction of wave travel with respect to the injector spuds, it is possible to determine the direction of the velocity perturbation which increases the burning rate. From this information, the sign of the radial velocity index for a given radial injector arrangement can be found.*

Several whole motor tests were made with the tangential spud orientation, using the injector of Figure 2 and the experimental aparatus described in Reference 1. Three pressure transducers were used to determine the direction or the wave travel with respect to the injector spuds. The results of four typical tests are shown in the following table:

Test No.	Chamber Diameter	Injection Diameter	Design MR	MR / Design MR	Mode	Direction
1	9	8	1.4	.90	1T	F → 0**
2	9	8	1.4	.87	2T	F → 0
3	6	5	2.2	.43	1T	F → 0
4	9	8	1.0	1.39	1T	F → 0

Considering the fuel-rich and oxidizer-rich zones as determined for this type of injector in Reference 9, the preferred direction was from oxidizer rich to fuel rich in agreement with the mechanism suggested above. Reference 5 discusses these tests in more detail.

The angle of the injection spray with respect to the combustion chamber axis is a function of the ratio of the test mixture ratio to the design mixture ratio, MR/design MR. If this ratio is less than one, the net lateral spray momentum is in the direction F → 0, and if it is greater than one, the spray momentum direction is 0 → F. It is clear from the test results that the wave travel direction was not affected by any rotation caused by off-design operation of the injector.

* This conclusion is true if the value of ℓ_θ is the same for all parts of the injector, as assumed in this study.

** The notation F → 0 refers to the order in which the spinning wave crosses the injector orifices.

It should be noted that although the operating conditions for tests 1 and 2 were very nearly the same, the resulting oscillations were of different modes. Moreover, from Figure 7 of Reference 1 (for $m_r = 1.4$ and $\alpha = 180^\circ$) it can be seen that the unstable mode of the standing type is the second tangential. The velocity effects for this configuration are illustrated by Figure 9. Although point "A", representing the test motor, is within only the second mode unstable zone for the standing form, it lies within both the first and second mode zones for the spinning form when velocity sensitivity is present. The difference between test 1 and 2 was in the starting period. Test 1 utilized the normal starting procedure, whereas an aluminum baffle was used in test 2. The effect of the baffle was to stabilize the first tangential mode during the first second of operation by constraining a standing mode oscillation pattern in the chamber. Upon burnout of the baffle, the oscillation changed to the spinning type without changing the mode. This result is an example of non-linear effects. Although for very samll oscillations both modes could co-exist, if the amplitudes are large one mode will dominate to the exclusion of the other. In this case the dominant mode will be the first tangential, unless the second tangential mode is allowed to grow to large amplitudes, as in test number 2.

The whole motor tangential orientation tests demonstrated that for the injector used in this investigation the burning rate is increased by a velocity perturbation in the direction $F \rightarrow 0$. A series of radial orientation angular stability limit tests was then made in which the arrangement of the injector was such that the direction $0 \rightarrow F$ was positive (outward). Therefore, a negative radial velocity was required to increase the burning rate, that is, the radial velocity index ℓ_r was negative. According to the velocity effect theory, as discussed above, for $\ell_r < 0$, the stability limits on the $n\tau$-plane are shifted toward smaller τ. It has also been shown that the

theoretical instability zones are moved in the direction of larger σ as the sector angle is increased. Thus, if the pressure interaction index and sensitive time lag are to be independent of the orientation of the injector spuds, the effect of the radial velocity must be counteracted by an increase in the sector angle. That is, the stability limits for the radial orientation should be at larger angles than those of the tangential orientation (no velocity effects).

This prediction was borne out by the radial orientation tests. Figure 10 shows the results for a typical configuration. The lower limit of the first tangential mode varied between approximately 90° and 120° over the range of mixture ratio, while the tangential orientation lower limit fell between 60 and 90°. From Figure 10 it can be seen that off-design operation with the radial orientation caused significant variation of the stability limits with mixture ratio, which may be due to distortion of the recirculation pattern.

The decreased stability of the spinning type of tangential modes due to tangential velocity effects was shown by a series of tests which utilized both a 180° sector motor and a whole (360°) motor with metal baffles. Such metal baffles were found to be capable of producing the same stable operation as the full 180° insert. It was also determined that stable operation resulted with a baffle only 5/8" long, if the baffle was placed against the injector face. When a space was left between the injector and baffle, instability was observed, even though a longer baffle was used. Thus, the tangential velocity ortangential displacement effects, which cause the spinning form to be much more unstable than the standing form, are concentrated near the injector face, in the early combustion zone.

In order to investigate the transition from the stable standing form of the tangential modes to the unstable spinning form, a destructible baffle was used. It was made of aluminum, 1/8" thick by 1" long, and was placed against

the injector face. Experiments showed that the aluminum baffle remained essentially intact for the first second of operation, but disappeared quickly at that time. Thus, each aluminum baffle test could show motor operation under both stable and unstable conditions.

A comparison of the stability of the standing and spinning modes using the tangential spud orientation is shown in Figure 11. The first and second lines represent the whole and half motor tests, respectively, which were discussed above. The third and fourth lines present the results of the aluminum baffle tests. It can be seen that the early portion of these tests corresponds to the 180° sector tests, and that as soon as the constraint to the standing mode was removed, the rocket operation became unstable. In the transition period a smooth increase in amplitude from the combustion noise level to that of the fully developed oscillation was observed. Data from a later series of tests, in which two transducers were used to determine the spin direction of this fully developed oscillation, are shown in Figure 12.

Further, more extensive experiments, using a 7" injection diameter to minimize chamber wall effects, showed that the direction of spin was dependent on mixture ratio (14). In whole motor tests it was found that at low mixture ratios the spin direction was opposite to that expected, whereas the predicted spin direction was observed at the design mixture ratio (1.4 in this case) and above. Similar results were obtained in tests using destructible baffles. Based on these results, it appeared that the locations of the regions of fuel- and oxidizer-rich composition change with mixture ratio because of variations in the impinging stream velocities.

In order to verify these suspected composition changes with mixture ratio, a separate flow study was made on the injector spuds. Using a Rupe-type sampling probe (15), simulating the liquid oxygen density with an appropriate sugar water solution, and substituting equivalent density RP-1 for

the water soluble alcohol, the data shown in Figure 13 were obtained. The low mixture ratio operation of the spud repeatedly indicated the presence of oxidizer-rich regions on the side of the spray toward the oxidizer hole. This contrasted with the reversed operation at design mixture ratio and above where the distribution followed the predictions of Reference 9.

Such behavior complicates experimental verification using the fuel-oxidizer impinging doublet type of injection. Therefore, a modified injection system was used to place fuel and oxidizer-rich zones in a fixed spatial relationship. Using two like-on-like doublets per spud, with a predetermined spacing between the resultant spray fans, as shown in Figure 12, it was possible to illustrate the preferential spin direction. Besides the inter-fan spacing, a radial spacing was inherent in the spud design because of manifolding requirements within the spud. The effect of this radial spacing (0.15 inch) was minimized by using 90° impinging streams so that a high degree of overlap (viewed tangentially) existed between fuel and oxidizer spray fans. Since this injection arrangement, using 0.1 inch spaced fans and operating at 150 psia, was basically stable, the destructible baffle (see Figure 14) was normally not used. However, where a small zone of spinning type instability did exist in the whole motor (as shown in Figure16), the baffle was employed during the starting transient to eliminate velocity effects.

The pulsing device used in these tests was the gun powder, pressure burst disc arrangement first used by Aerojet (15). Thus, the ordinate in Figures 15 and 16 is specified in grains of pistol powder and burst disc pressure in thousands of pounds. Although this will suffice for the discussions here, nonlinear limits of instability must be related to the more fundamental quantities such as pressure and velocity. Such data are presented in Reference 14 and 17.

The experimental program included tests in which the pulse direction was from oxidizer to fuel (the predicted preferential direction) and tests with pulses in the opposite direction. Consider first the results of pulsing in the preferred direction, oxidizer to fuel (denoted by $\bar{O} \rightarrow F$, where the bar indicates that the oxidizer spray is closest to the chamber wall) shown in Figure 15. Except for one extraordinary test with the whole motor, all of the unstable tests with this arrangement were found to be spinning in the $\bar{O} \rightarrow F$ direction (i.e., the same direction as the initial pulse).

Perhaps a better test for verifying the directional aspect of the velocity effect is presented in the data shown in Figure 16. Here the position of fuel and oxidizer spray fans has been reversed. Therefore, the pulse direction ($\bar{F} \rightarrow O$) is opposite to that theoretically preferred. However, the final spin direction of the unstable combustion remains $O \rightarrow \bar{F}$. It is interesting to observe the sequence of events which lead to this result. Figure 17 shows the time history of a typical pulsed test with this configuration. The imparted pulse disturbance ($\bar{F} \rightarrow O$) in this case persists less than 20 milliseconds and is followed by a brief period of standing mode instability. The latter transforms to $O \rightarrow \bar{F}$ spinning mode oscillations, gradually building to maximum amplitude. Thus, the preference for the $O \rightarrow F$ direction is clearly shown.

It must be remembered, however, that even with only a 0.1 inch spacing, the like-on-like arrangement can only roughly approximate the uniform change from fuel-rich to oxidizer-rich composition assumed in the theory. With wider spacing this linear assumption could not be expected to apply and nonlinear formulation of the velocity effect is currently in progress at Princeton.

REFERENCES

1. Crocco, L., Harrje, D. T., and Reardon, F. H., "Transverse Combustion Instability in Liquid Propellant Rocket Motors" ARS Journal, March 1962, Vol. 32, No. 3, PP 366-373.

2. Crocco, L., and Cheng, S. I., "Theory of Combustion Instability in Liquid Propellant Rocket Motors," Agardograph No. 8, Butterworths Scientific Pub., Ltd., London, 1956.

3. Scala, S. M., "Transverse Wave and Entropy Wave Combustion Instability in Liquid Propellant Rockets," Princeton University (Ph.D. Thesis), Aeronautical Engineering Report No. 380, April 1, 1957.

4. Crocco, L., Grey, J., and Harrje, D. T., "Theory of Liquid Propellant Rocket Combustion Instability and Its Experimental Verification," ARS Journal, Vol. 30, No. 2, February 1960.

5. Reardon, F. H., "An Investigation of Transverse Mode Combustion Instability in Liquid Propellant Rocket Motors," Princeton University (Ph.D. Thesis), Aeronautical Engineering Report No. 550, 1 June 1961.

6. Levine, R., and Bambanek, R., "A Sustaining Mechanism for a Transverse Mode of Combustion Instability," Rocketdyne Report No. R-326, 13 Nov. 1956. (Confidential)

7. Peoples, R. G., and Pickford, R. S., "Analytical and Experimental Scaling of Thurst Chambers," Aerojet-General TN-40 (AFRSR677), November 1960.

8. Wieber, Paul R., and Mickelsen, William, "Effect of Transverse Acoustic Oscillation on the Vaporization of a Liquid-Fuel Droplet," NASA TN D-287, May, 1960.

9. Somogyi, D., and Feiler, C.B., "Mixture Ratio Distribution in the Drops of Spray Produced by Impinging Liquid Streams," ARS Journal, Vol.30, No. 2, February 1960, pp. 185-187.

10. Priem, Richard J., and Heidmann, Marcus F., "Propellant Vaporization as a Design Criterion for Rocket-Engine Combustion Chambers," NASA TR R-67, 1960.

11. Pass, Isaac, and Tischler, Adelbert O., "Effect of Fuels on Screaming in 200-Pound-Thurst Liquid-Oxygen-Fuel Rocket Engine," NACA RM E56 C 10 June 22, 1956.

12. Courant, R., and Hilbert, D., "Methods of Mathematical Physics." Vol. I Interscience Publishers Inc., New York, 1953.

13. Kantorvich, L. V., and Krytov, V. I., "Approximate Methods of Higher Analysis," P. Noordnoff, Ltd. - Groningen, The Netherlands, 1958.

REFERENCES (CONT.)

14. Crocco, L., Harrje, D. T., Strahle, W. C. and Sirignano, W. A., "Nonlinear Aspects of Combustion Instability in Liquid Propellant Rocket Motors", Princeton University Aeronautical Engineering Report No 553b, 1 June 1962.

15. Rupe, J. H., "The Liquid Phase Mixing of a Pair of Impinging Streams" Progress Report No. 20-195, J. P., L., Aug 6, 1953.

16. Krieg, H. C. Jr., "The Tangential Mode of Combustion Instability", ARS Preprint, No. 1723-61, Palm Beach, Florida, April 1961.

17. Crocco, L., Harrje, D. T., Lee, D. H., Strahle, W. C., Sirignano, W. A., Bredfeldt, H. R., Seebaugh, W. R., "Nonlinear Aspects of Combustion Instability in Liquid Rocket Motors", Princeton University Aeronautical Engineering Report No. 553c, 1 June 1963.

TITLES FOR FIGURES

Figure 1. Standing and spinning forms of the first tangential modes.

Figure 2. Doublet spud orientation and design.

Figure 3. Effect of spud orientation observed in transverse instability tests using a 9 inch diameter combustion chamber and an 8 inch injection circle diameter.

Figure 4. Schematic representation of the fuel and oxidizer-rich stratification produced by a doublet spud.

Figure 5. Typical solution for the combustion parameters n (ω) and $\tau(\omega)$

Figure 6. Stable and unstable regions on the n, τ -plane.

Figure 7a. Theoretical tangential velocity effect on stability limits, first tangential mode, uniformly distributed combustion; chamber exit Mach No., $\bar{u}$ = 0.10.

Figure 7b. Theoretical tangential velocity and displacement sensitivity for the first tangential mode, ℓ_r = 0, same conditions as in Figure 7a.

Figure 8a. Theoretical radial velocity effect on stability limits, first tangential mode, uniformly distributed combustion; chamber exit Mach number, $\bar{u}_e$ = 0,10

Figure 8b. Theoretical radial velocity and displacement sensitivity for the first tangential mode, ℓ_θ = 0, same conditions as in Figure 8a.

Figure 9. Theoretical predictions of the tangential velocity effect with combustion concentrated at an injection diameter circle of 8 inches in a 9 inch diameter chamber, r_i = 8/9; $\bar{u}_e$ = 0.05

Figure 10. Shift of stability limits due to radial velocity effects in a 9 inch diameter sector motor with 8 inch diameter injection circle operated at 150 psia chamber pressure (nominal thrust 1,000 lbs, alcohol-oxygen)

Figure 11. Tangential spud orientation baffle tests using a 6 inch diameter chamber with 5 inch diameter injection circle, 150 psia chamber pressure and nominal thrust at 500 lbs., alcohol-oxygen.

Figure 12, Linear instability buildup following baffle burnout as recorded on two pressure transducers mounted at 90° on the chamber wall using a 9 inch chamber diameter, 7 inch injection circle diameter, 150 psia chamber pressure and a 1,000 lb. nominal thrust, alcohol oxygen.

Figure 13. Mixture ratio gradients across the spray fan of a fuel-on-oxidizer impinging doublet spud, orifice diameter .081-inches.

Figure 14. Chamber arrangement for investigating shock pulse effects on stability limits including a typical run time sequence.

Figure 15. Pulsed limits testing of an injection composed of .1 inch spacing, like-on-like spuds using a 9 inch diameter injector, 7 inch injection circle diameter, 150 psia chamber pressure and 1,000 lb. nominal thrust. Pulses directed $\bar{O} \rightarrow F$ (oxidizer outside).

Figure 16. Same test conditions as Figure 15 but pulse directed $\bar{F} \rightarrow O$ (fuel outside).

Figure 17. Pressure records indicating the preferred tangential mode spin direction under the conditions noted for Figure 16.

TABLE I

Velocity Effect Coefficients for Uniform Injection, Full Circular Chamber

Mode	ν	h	$\frac{B_{\nu h}}{\delta_{\nu h}}$	$\frac{\tilde{C}_{\nu h}}{S_{\nu h}}$	(spinning mode)
First tangential	1	1	0.19116	0.77402	
Second tangential	2	1	0.18124	0.85258	
First radial	0	2	-0.13320	0.00000	
First combined	1	2	0.02884	0.22197	

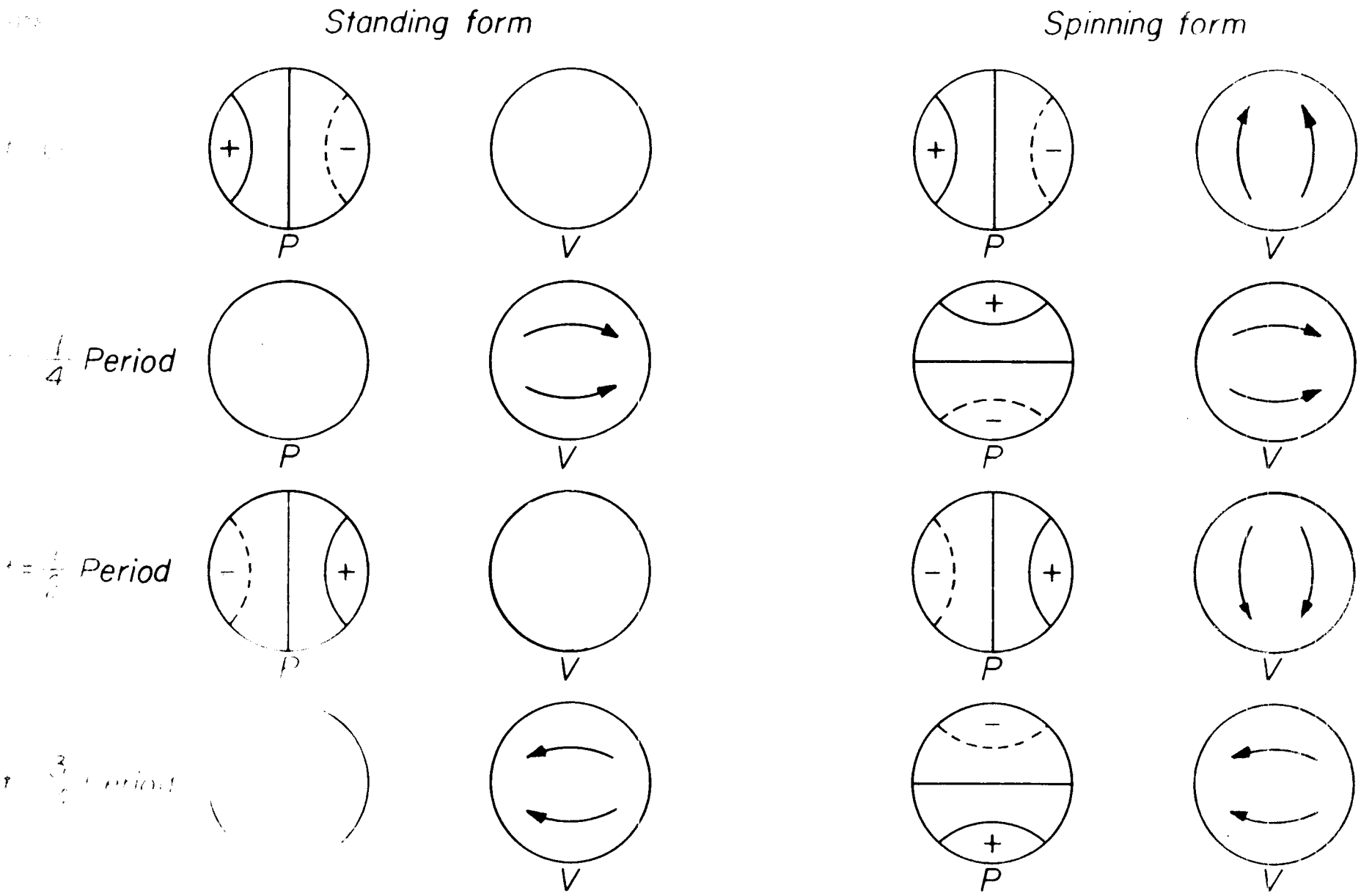
Standing form
Spinning form
+
−
P
V
1/4 Period
1/2 Period
3/4 Period

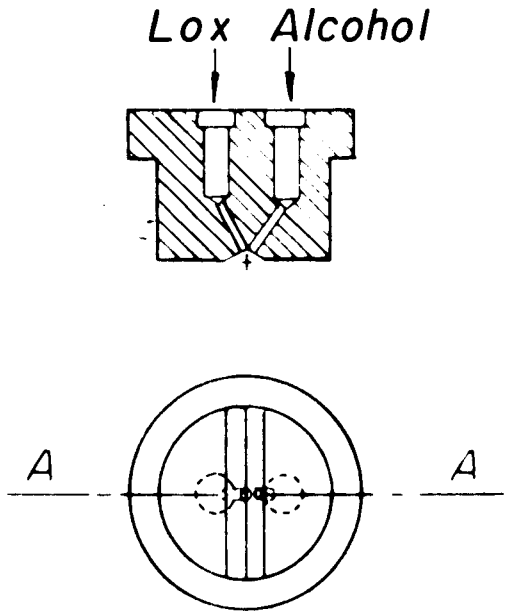

A-A = Line of centers of injection holes

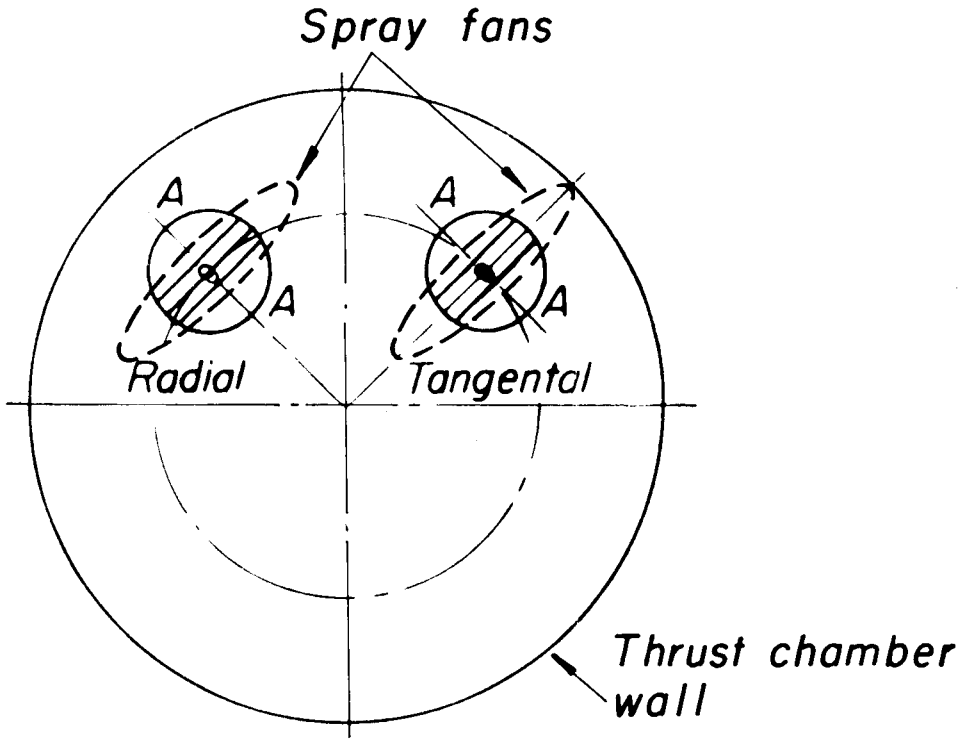

Spud orientation

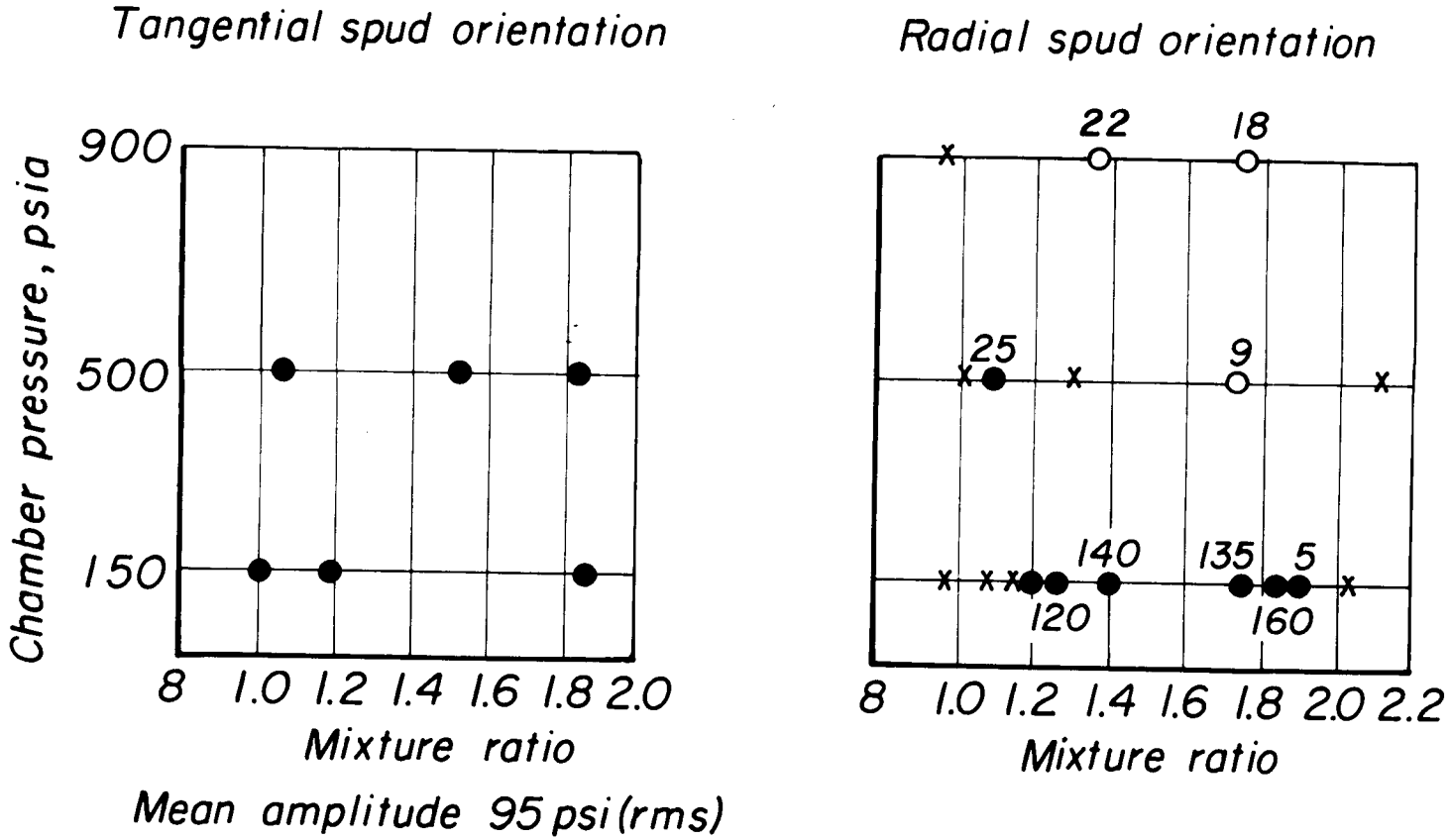

Key: x - stable, ● - first tangential mode, ○ - second tangential mode
Numbers over symbols indicate amplitude psi, pk-to-pk

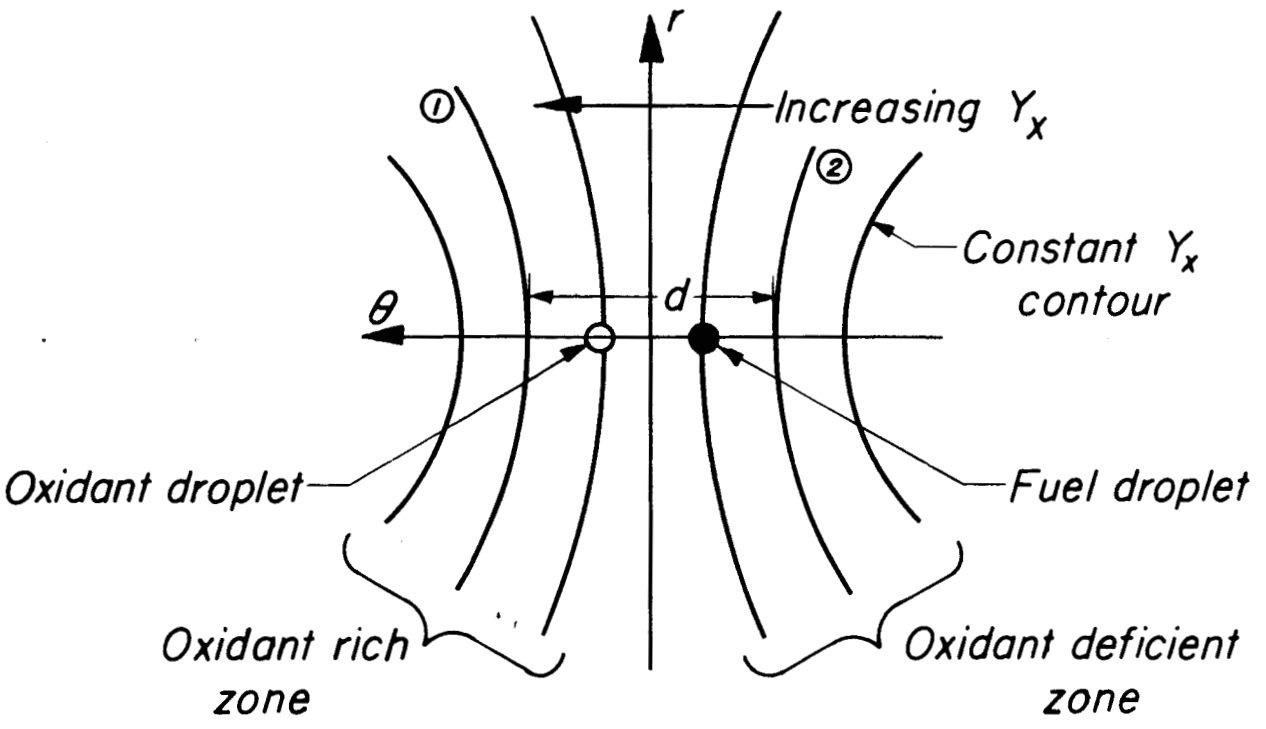

(a) Spray produced by tangentially oriented injector spud

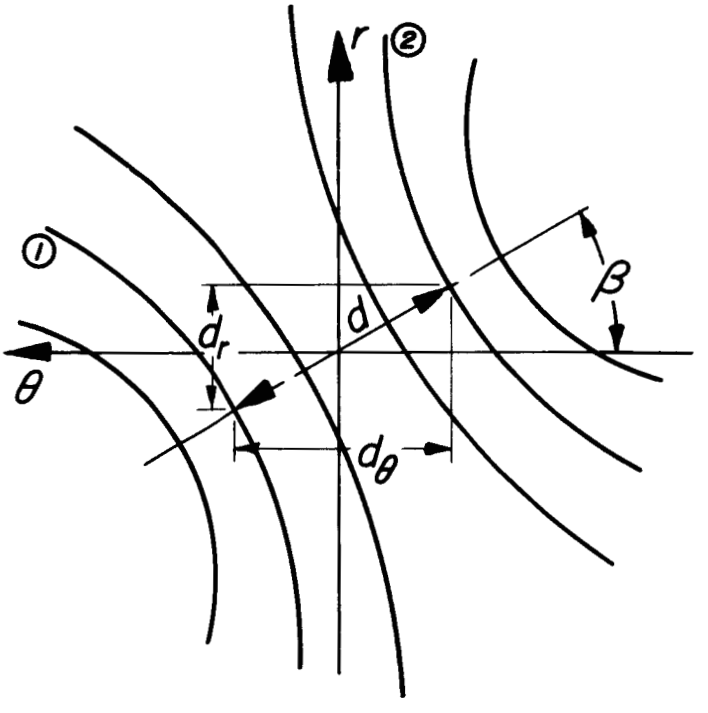

(b) Spray produced by rotated spud

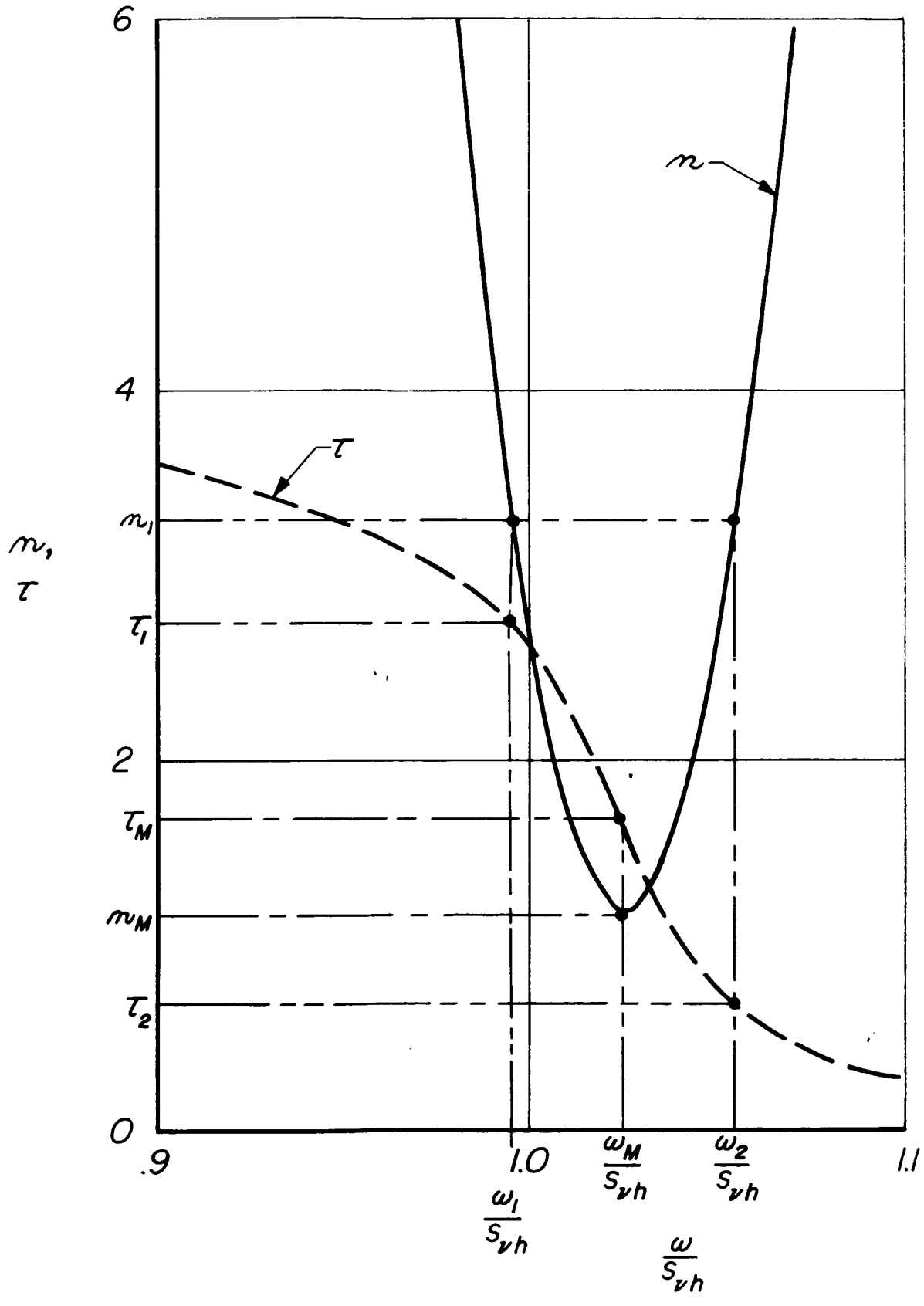
6
4
2
0
n
τ
n₁
τ₁
τ_M
n_M
τ₂
n, τ
.9
1.0
1.1
ω_M / S_νh
ω_2 / S_νh
ω_1 / S_νh
ω / S_νh

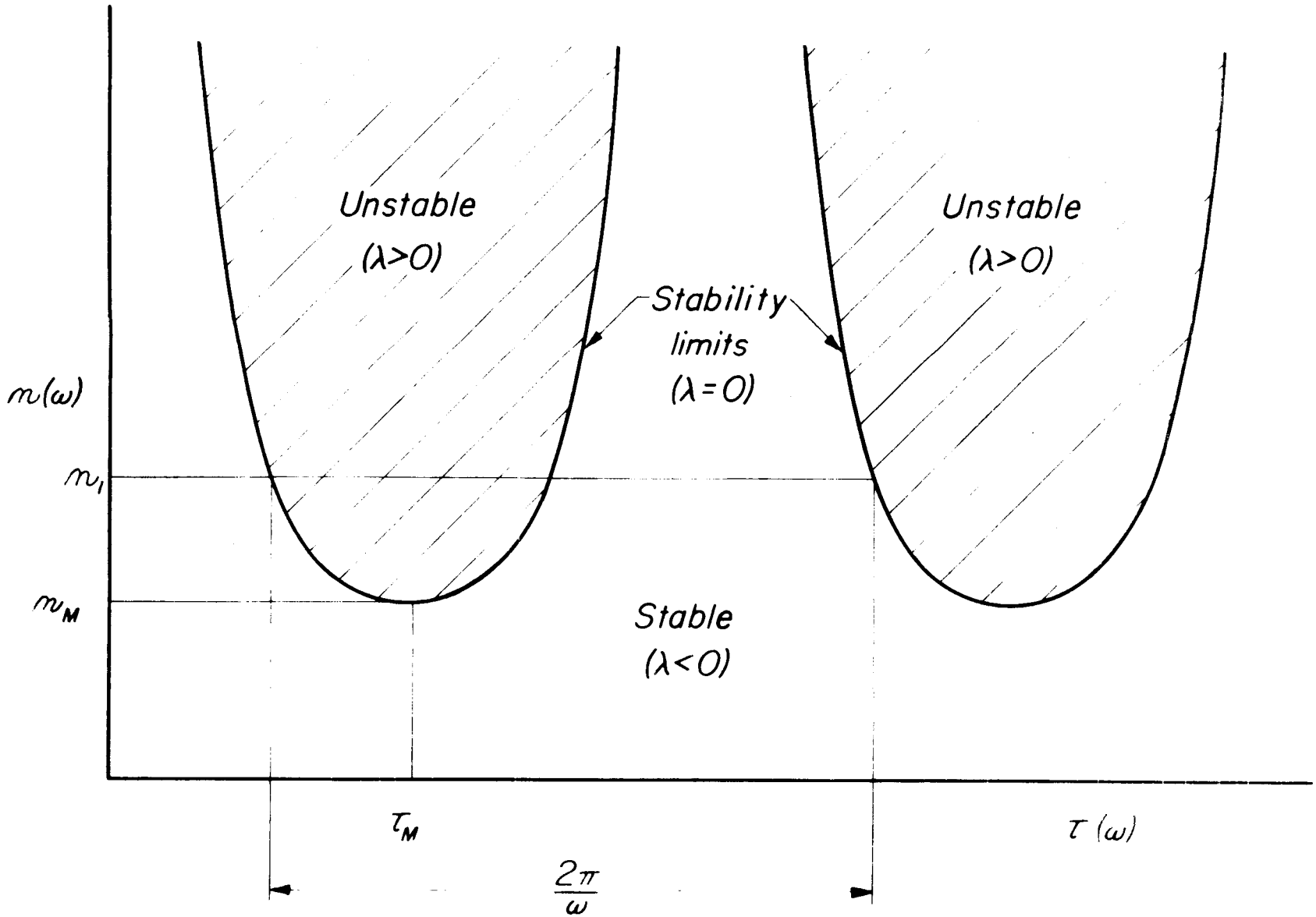
Unstable
(λ>0)
Stability
limits
(λ=0)
Unstable
(λ>0)
n(ω)
n1
nM
Stable
(λ<0)
τM
τ(ω)
2π/ω

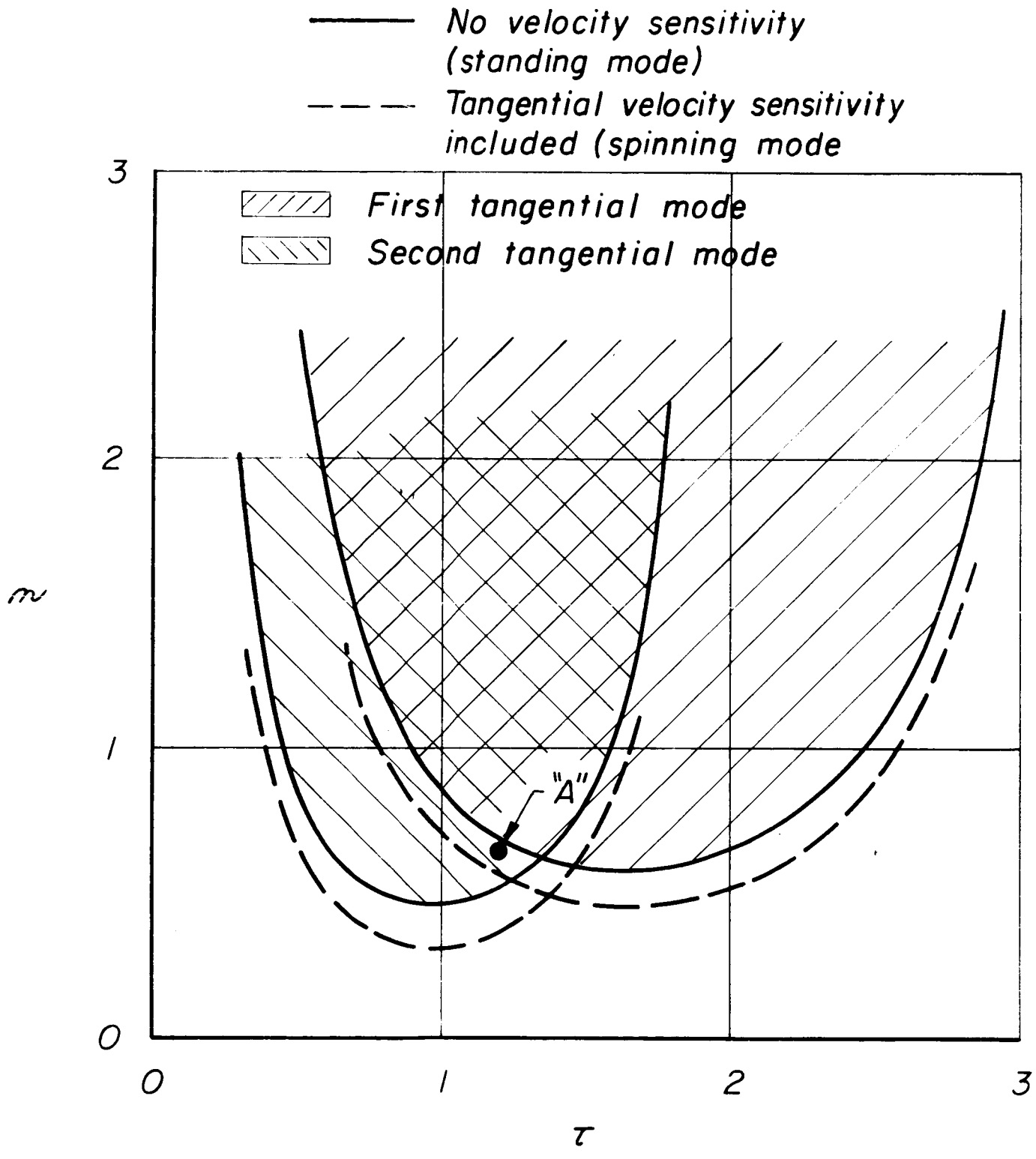
No velocity sensitivity
(standing mode)
Tangential velocity sensitivity
included (spinning mode
First tangential mode
Second tangential mode
"A"
3
2
1
0
0
1
2
3
n
τ

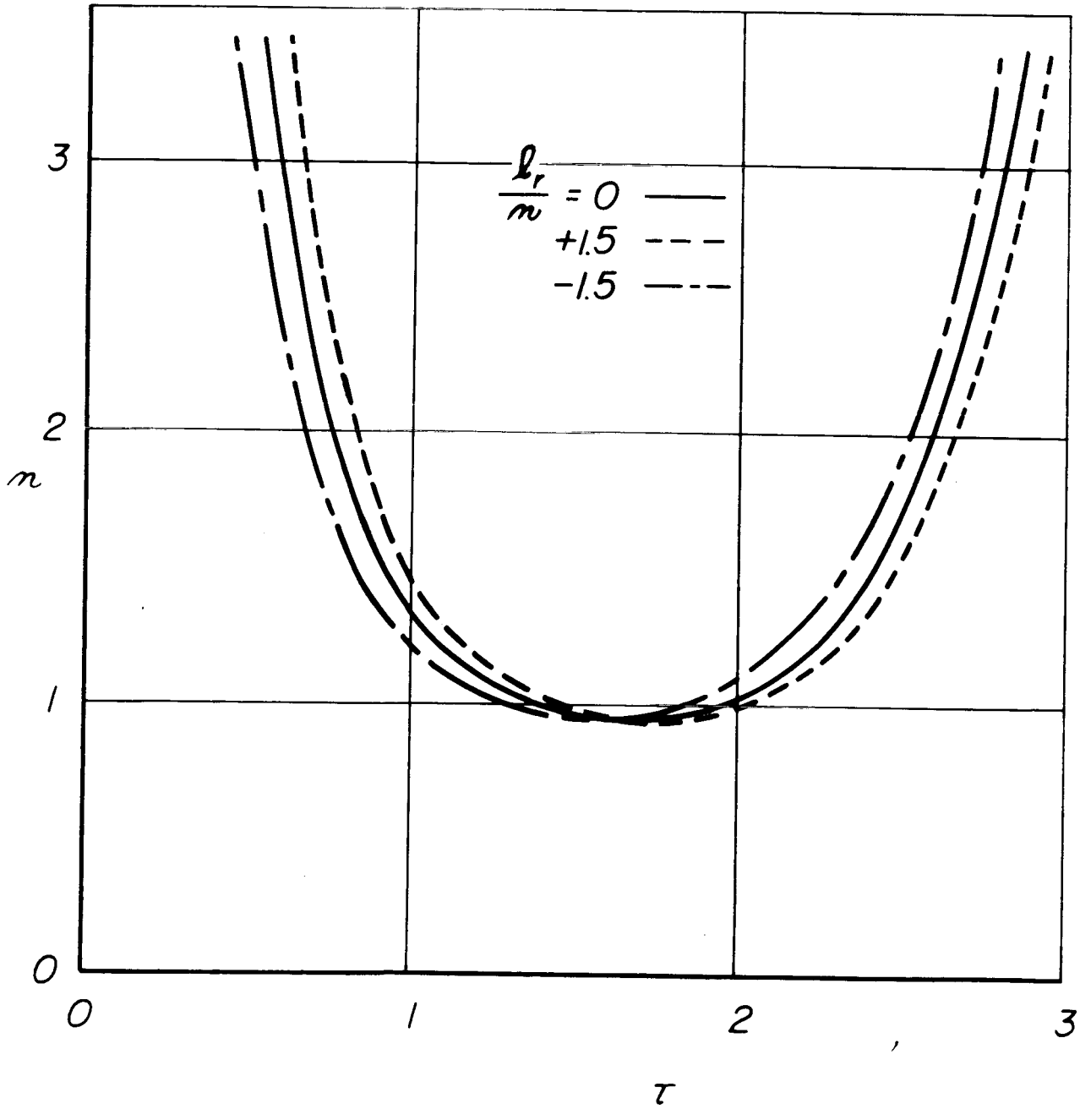

JPR 853

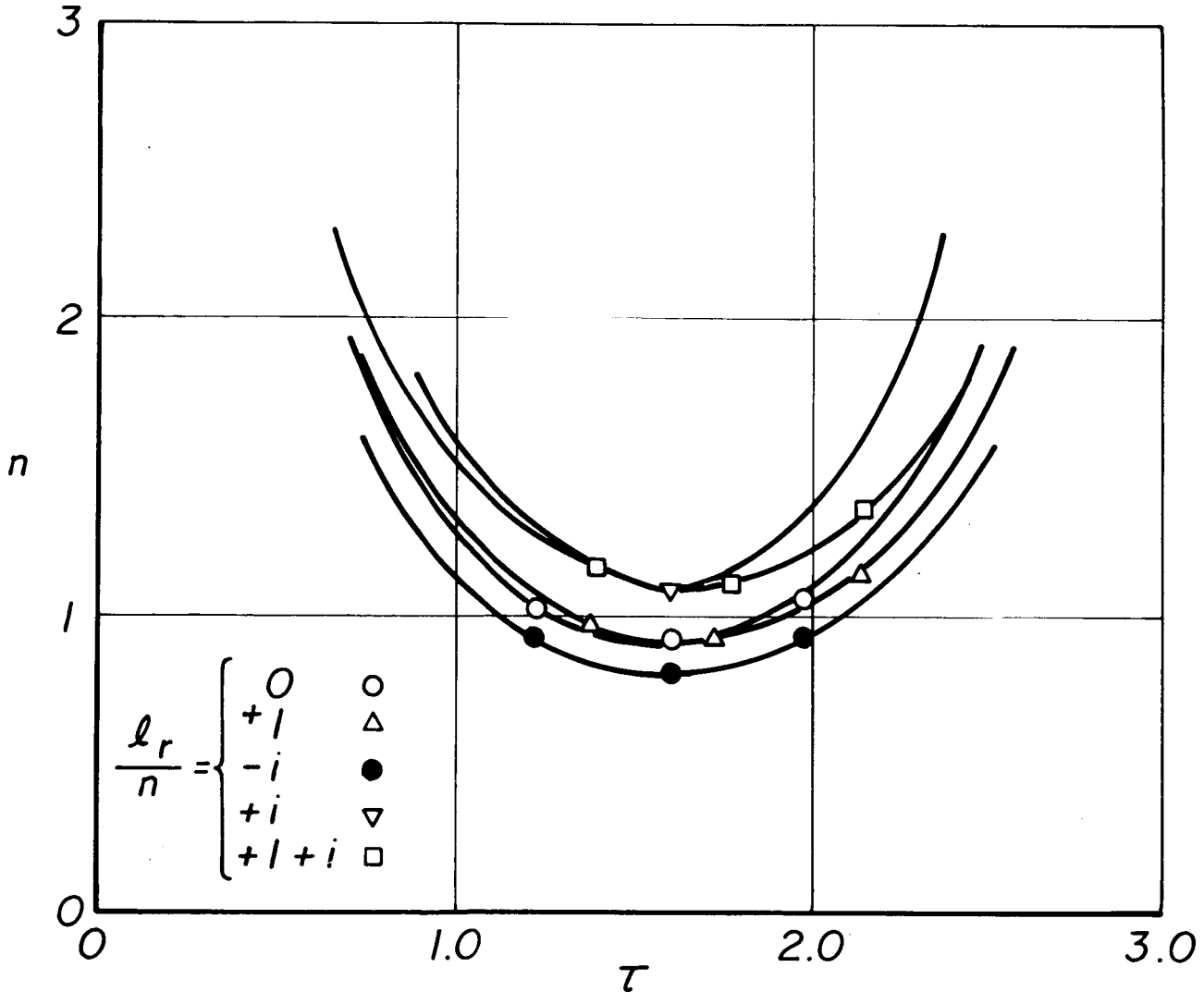
3
2
1
0
n
0
1.0
2.0
3.0
τ
$\frac{\ell_r}{n}$ = { 0 ○ ; +1 △ ; −i ● ; +i ▽ ; +1 +i □

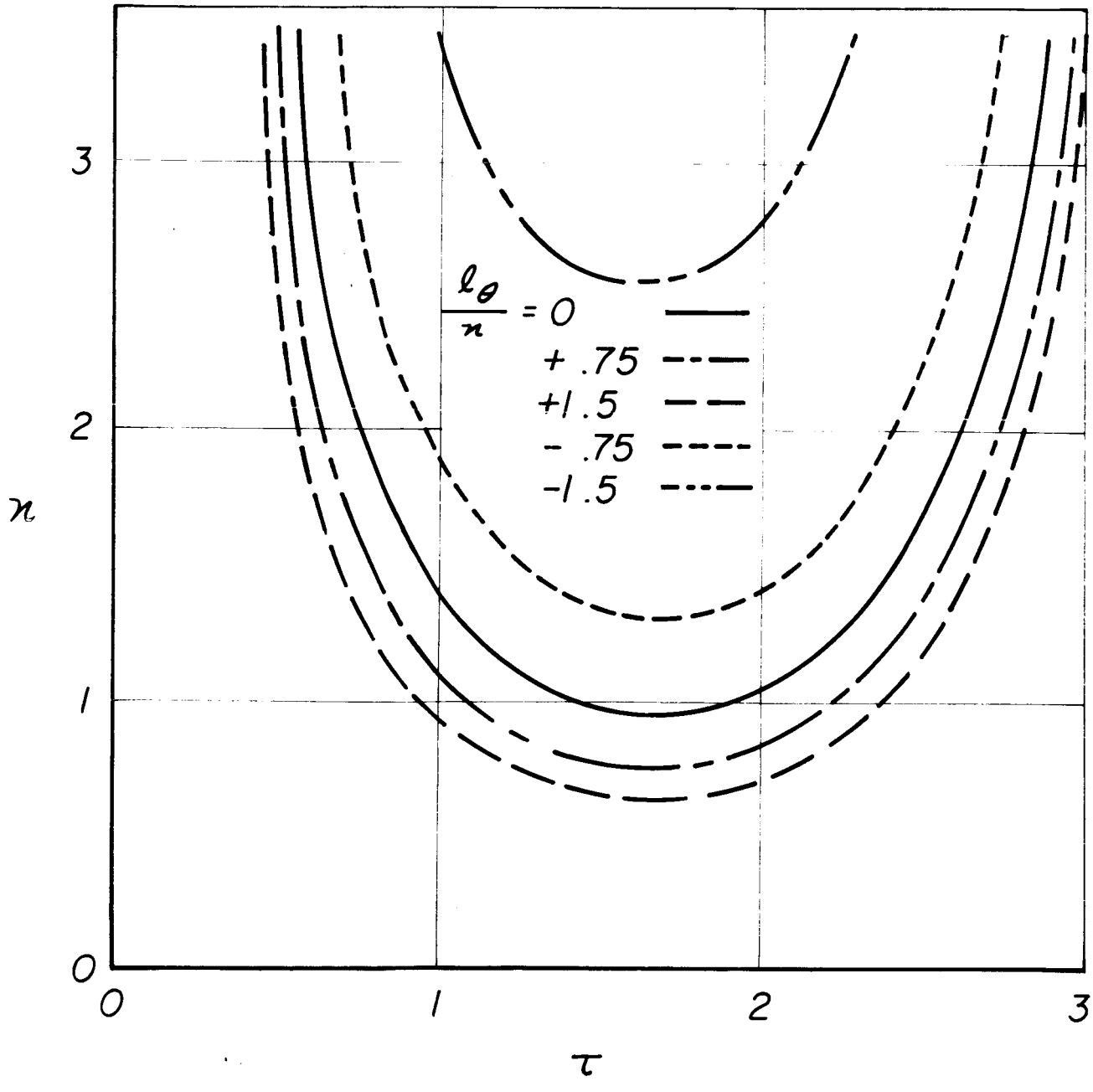

851

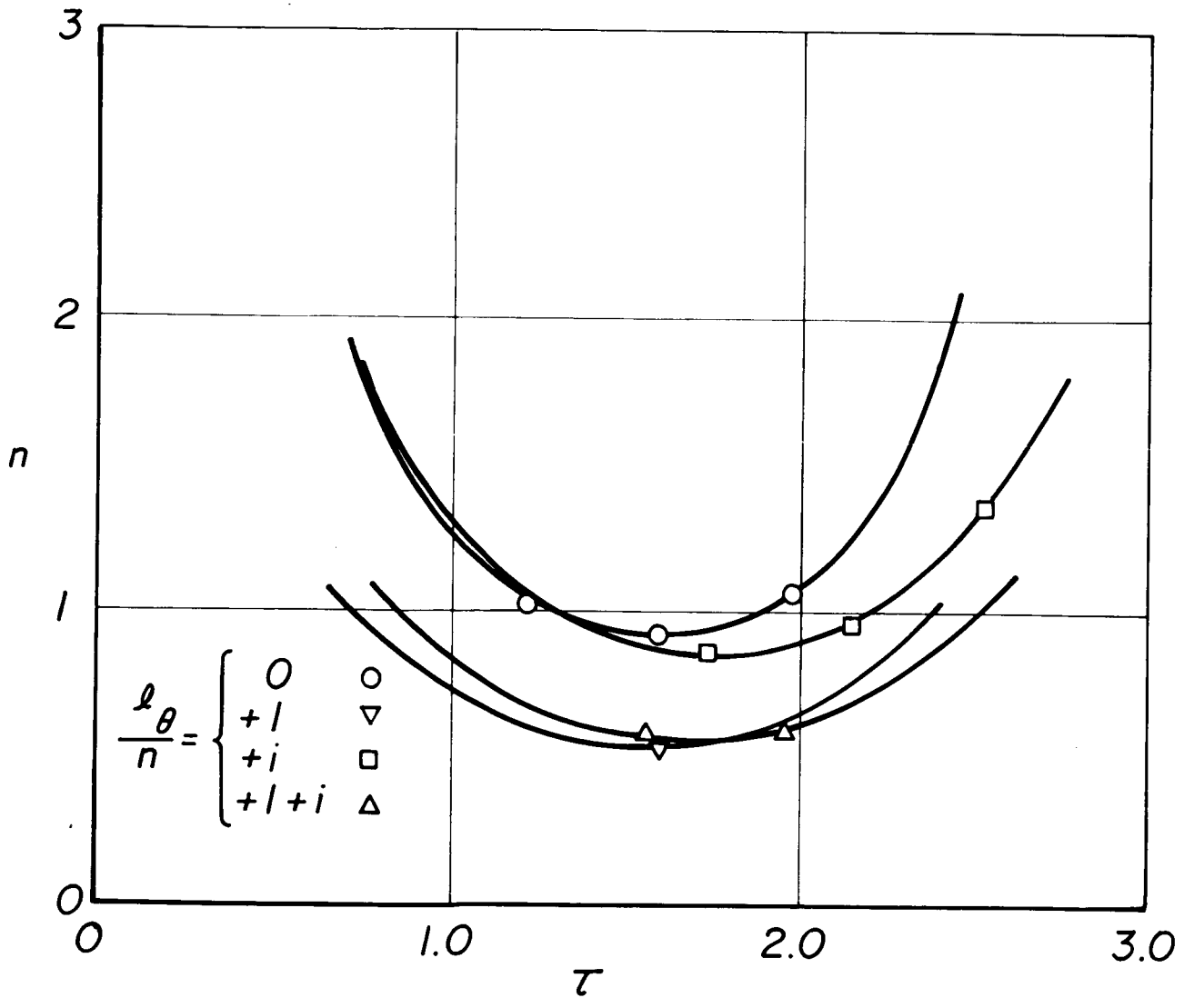
3
2
1
0
n
0
1.0
2.0
3.0
τ
$\frac{\ell_\theta}{n}$ = { 0 ○ ; +1 ▽ ; +i □ ; +1+i △

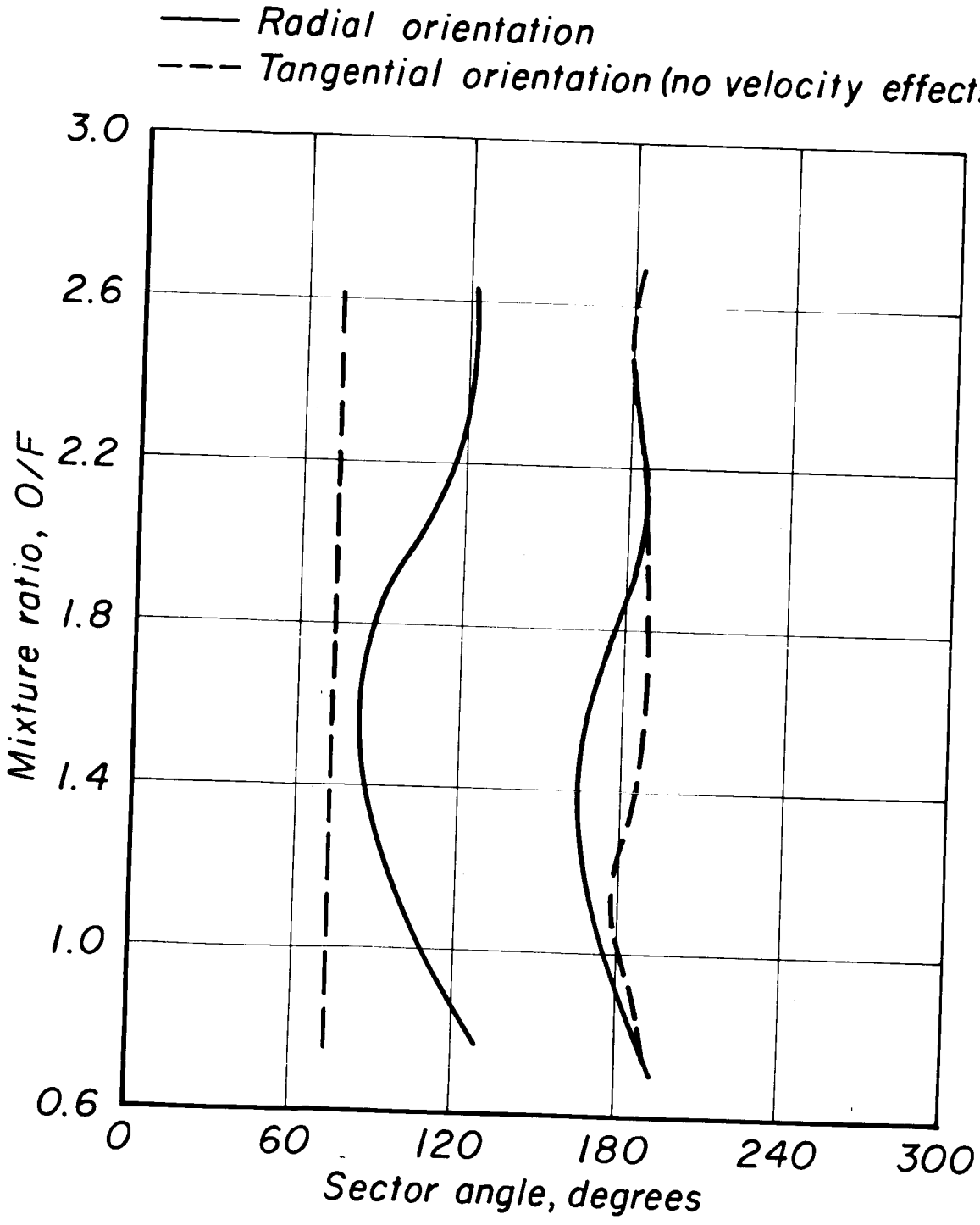
Radial orientation
Tangential orientation (no velocity effects)
3.0
2.6
2.2
1.8
1.4
1.0
0.6
Mixture ratio, O/F
0
60
120
180
240
300
Sector angle, degrees

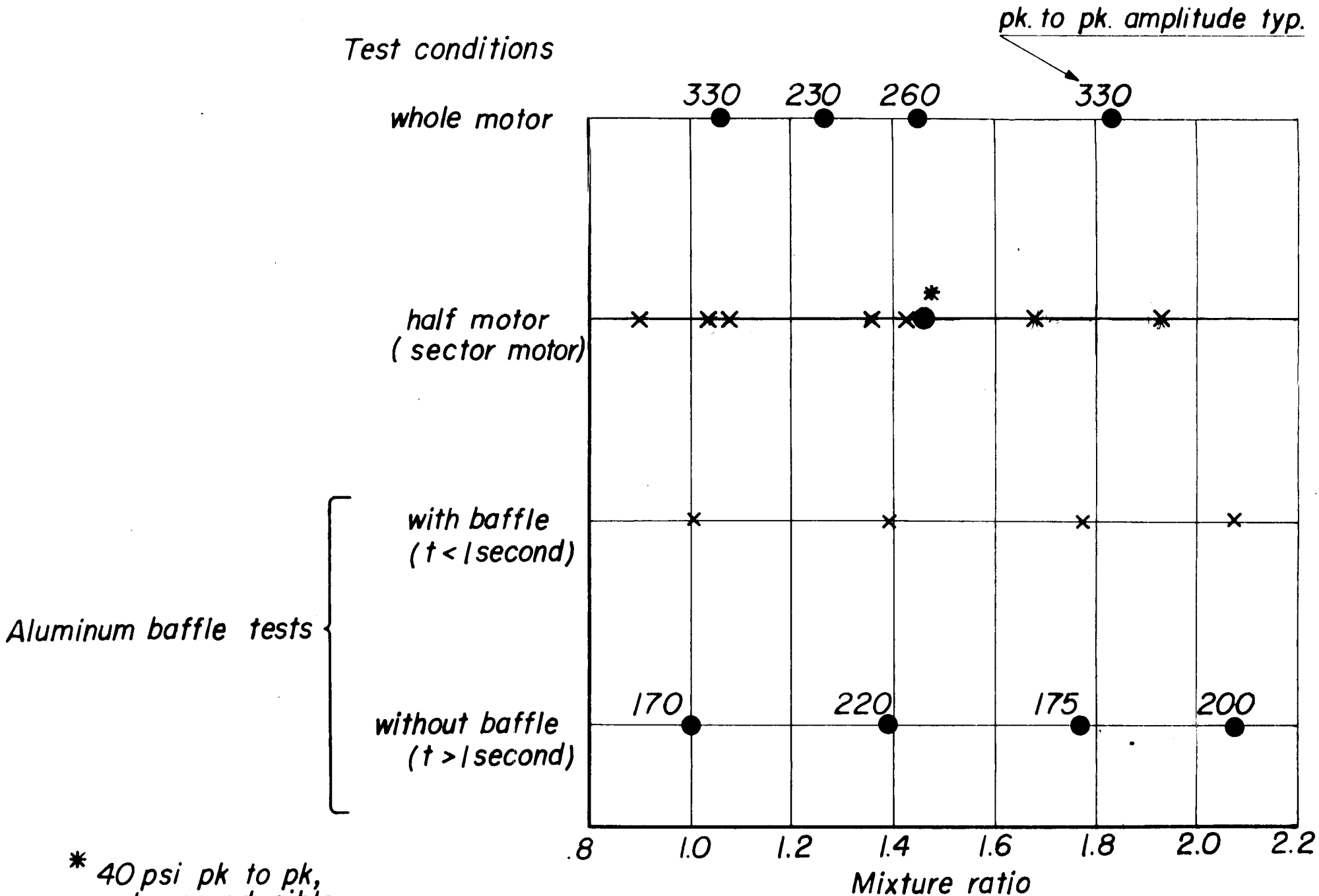
pk. to pk. amplitude typ.
Test conditions
330
230
260
330
whole motor
half motor
(sector motor)
with baffle
(t < 1 second)
Aluminum baffle tests
without baffle
(t > 1 second)
170
220
175
200
.8
1.0
1.2
1.4
1.6
1.8
2.0
2.2
Mixture ratio
* 40 psi pk to pk, not reproducible

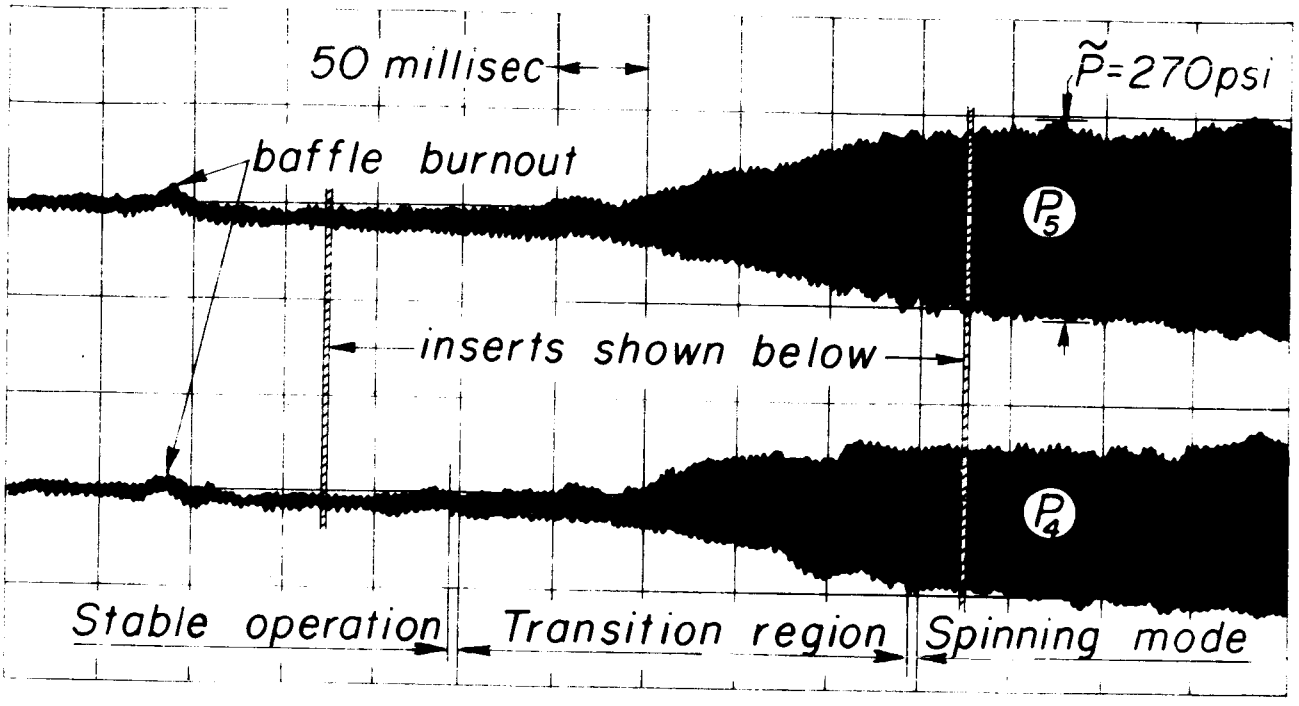

Stability record after baffle burnout

time →

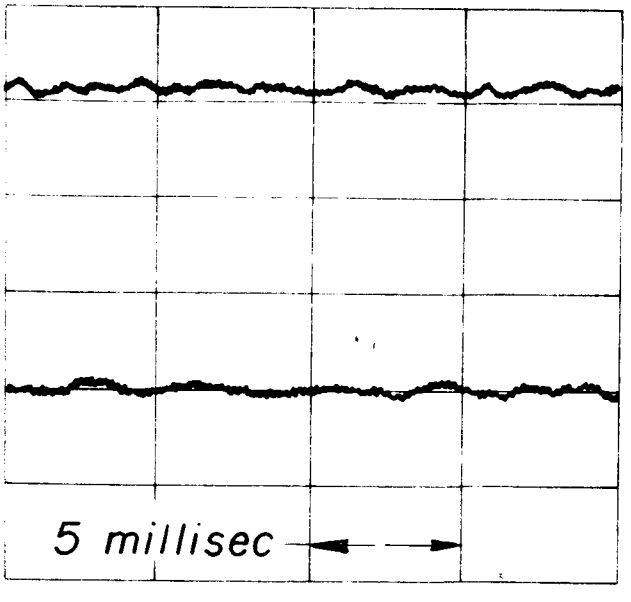

Stable operation

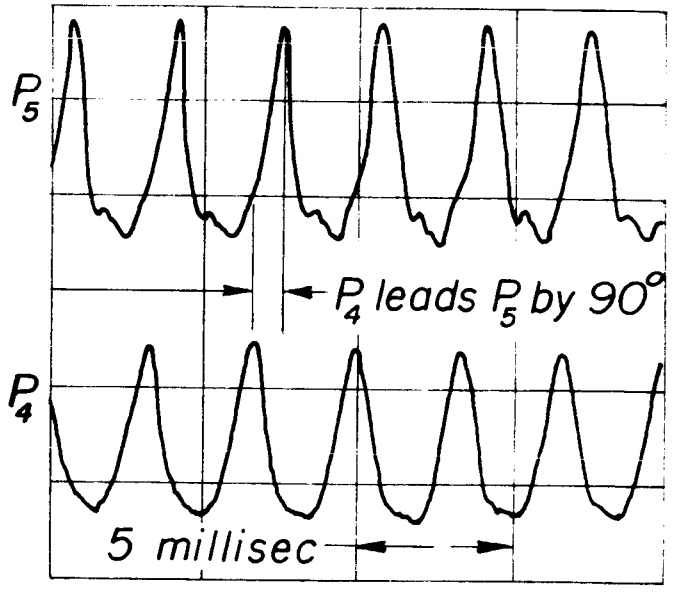

Spinning first tangential mode

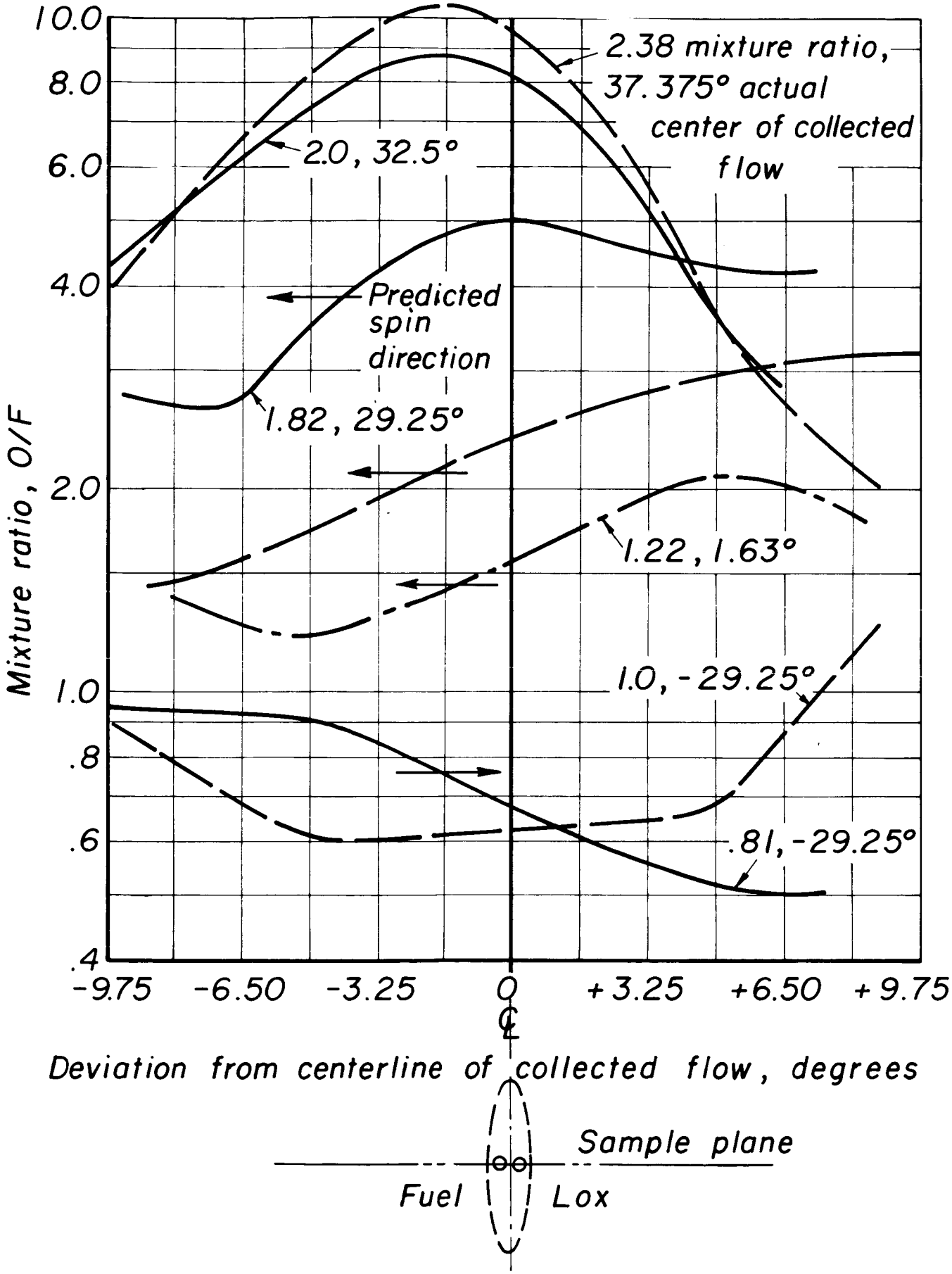
10.0
8.0
6.0
4.0
2.0
1.0
.8
.6
.4
Mixture ratio, O/F
2.38 mixture ratio,
37.375° actual
center of collected
flow
2.0, 32.5°
Predicted
spin
direction
1.82, 29.25°
1.22, 1.63°
1.0, -29.25°
.81, -29.25°
-9.75
-6.50
-3.25
0
+3.25
+6.50
+9.75
℄
Deviation from centerline of collected flow, degrees
Sample plane
Fuel
Lox

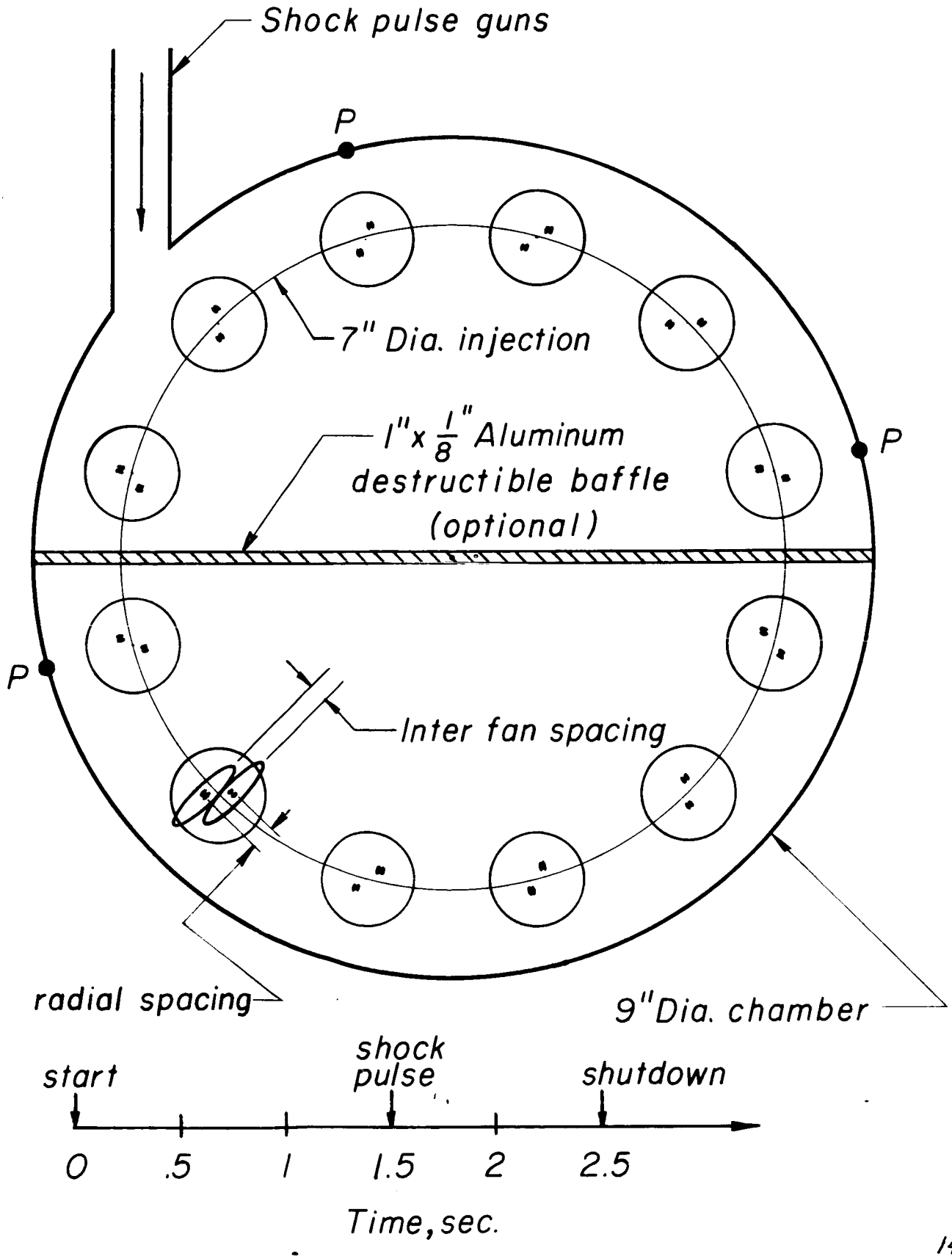
Shock pulse guns
P
7" Dia. injection
1"x 1/8" Aluminum
destructible baffle
(optional)
P
P
Inter fan spacing
radial spacing
9" Dia. chamber
start
shock
pulse
shutdown
0
.5
1
1.5
2
2.5
Time, sec.

JPR 1220

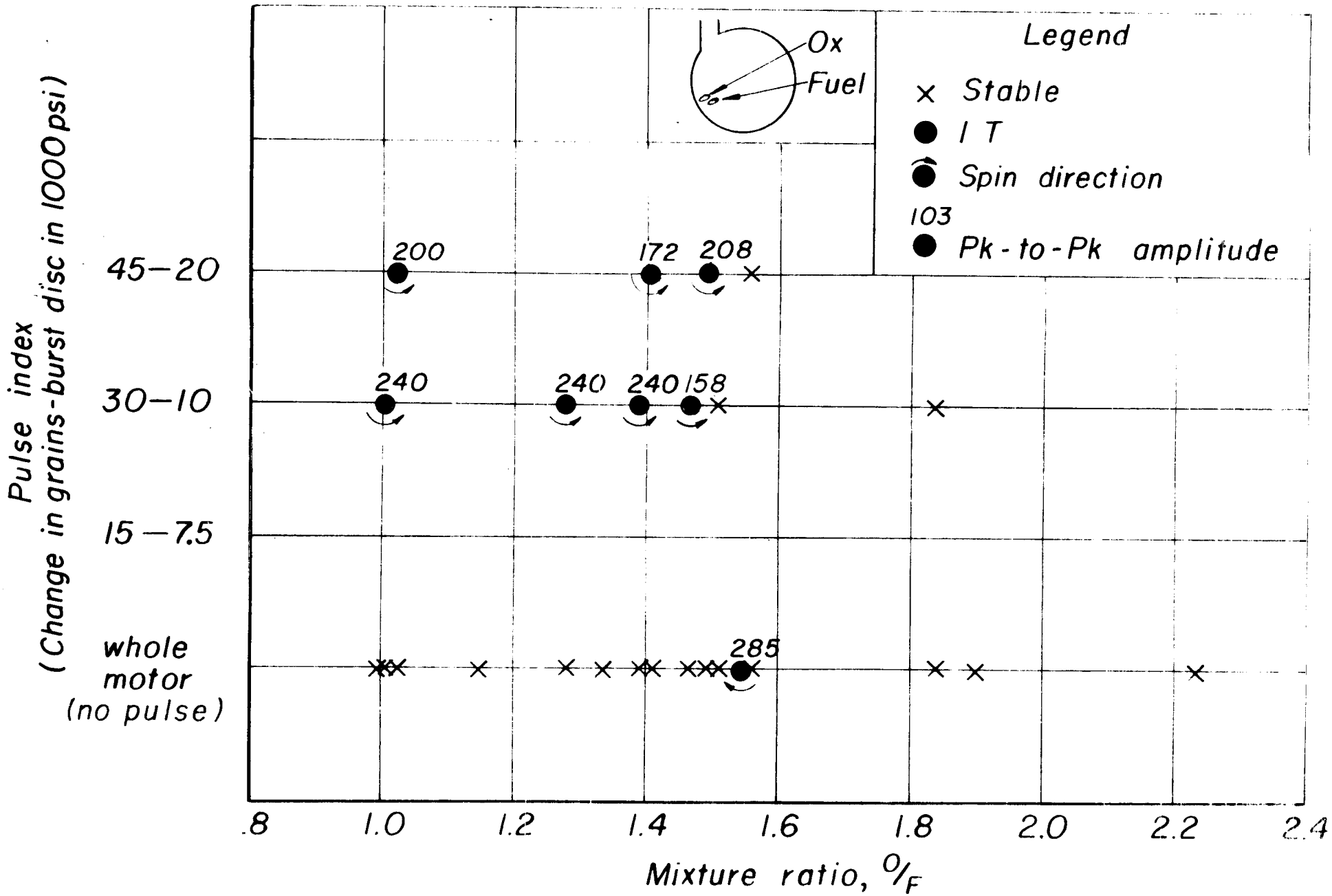
Ox
Fuel
Legend
Stable
I T
Spin direction
103
Pk - to - Pk amplitude
200
172
208
240
240
240
158
285
45–20
30–10
15–7.5
whole motor (no pulse)
Pulse index (Change in grains-burst disc in 1000 psi)
.8
1.0
1.2
1.4
1.6
1.8
2.0
2.2
2.4
Mixture ratio, O/F

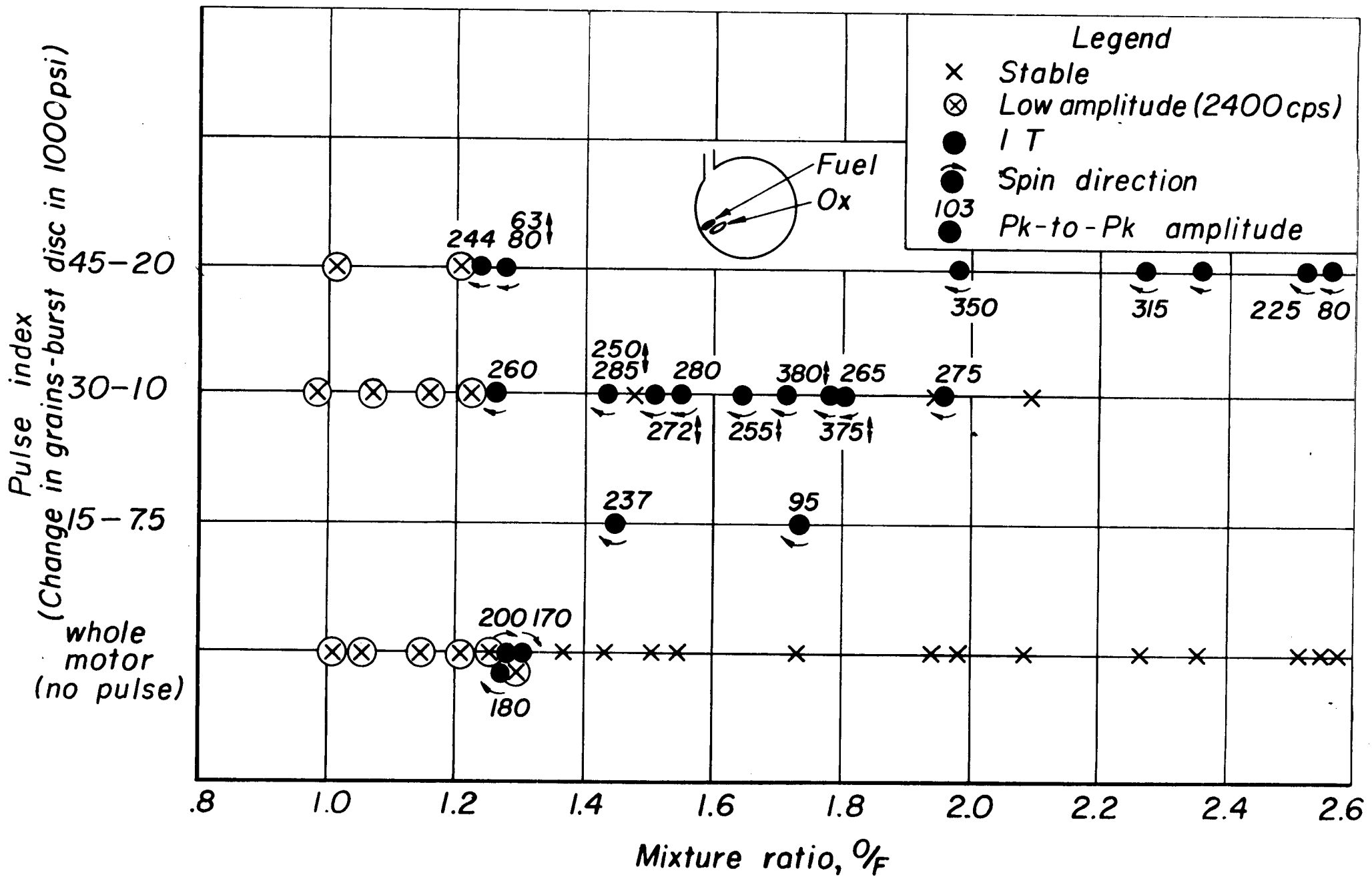
Legend
Stable
Low amplitude (2400 cps)
I T
Spin direction
Pk-to-Pk amplitude
Fuel
Ox
Pulse index
(Change in grains-burst disc in 1000 psi)
45–20
30–10
15–7.5
whole motor (no pulse)
244
63
80
350
315
225
80
103
260
250
285
280
272
380
265
255
375
275
237
95
200
170
180
.8
1.0
1.2
1.4
1.6
1.8
2.0
2.2
2.4
2.6
Mixture ratio, O/F

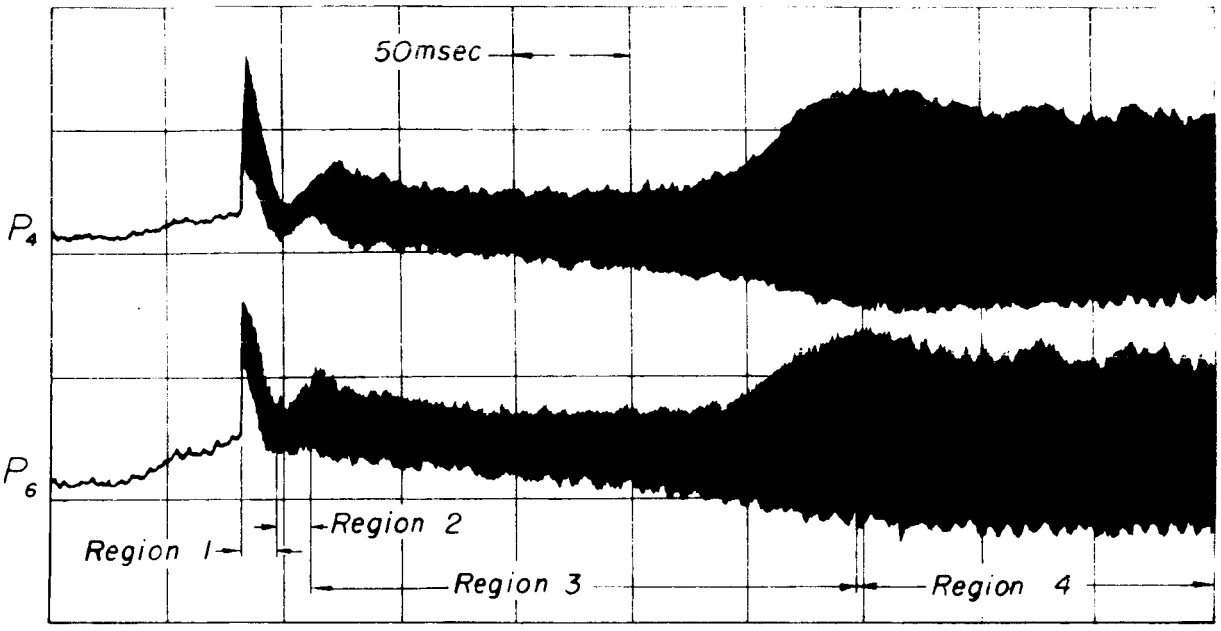

Nonsteady pressure recorded on two pressure transducers (spaced at 90°) for a fuel to oxidizer oriented pulse supplied by a 30 grain charge and 10,000 lb burst disc

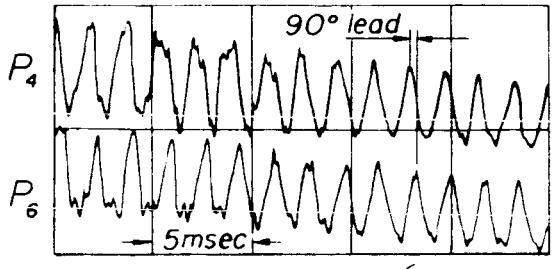

Region 1 - Pulse disturbance, Spinning wave

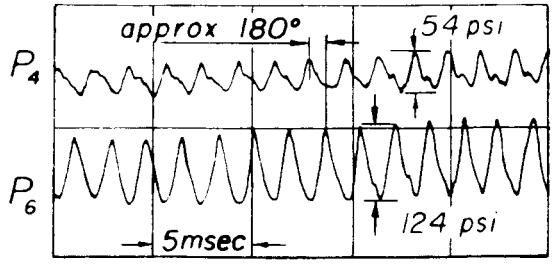

Region 2 - Standing wave pattern

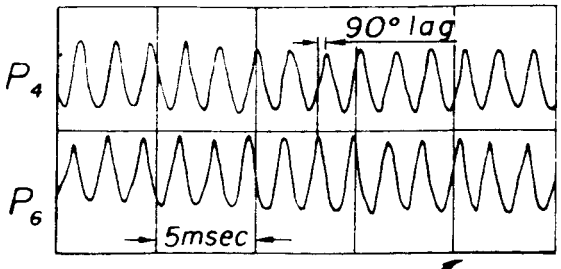

Region 3 - Increasing amplitude, Spinning wave

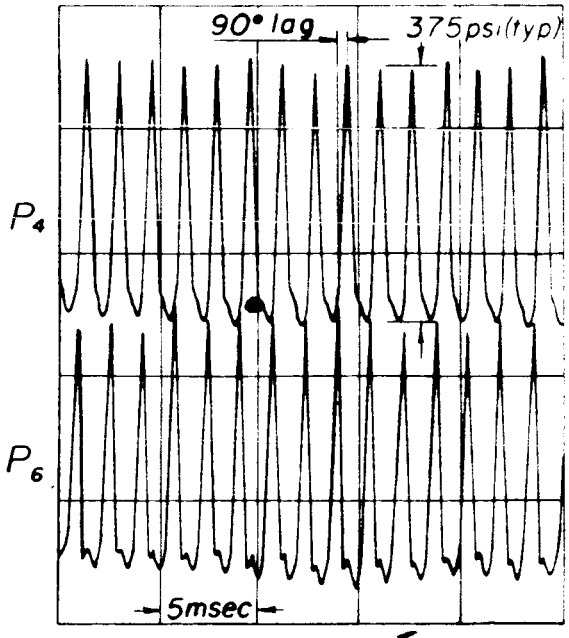

Region 4 - Full amplitude, Spinning wave